



A highly homogeneous polymer composed of tetrahedron-like monomers for high-isotropy expansion microscopy

Ruixuan Gao^{1,2,3,17}, Chih-Chieh (Jay) Yu^{1,2,4,17}, Linyi Gao^{2,4,5}, Kiryl D. Piatkevich^{1,2}, Rachael L. Neve⁶, James B. Munro⁷, Srigokul Upadhyayula^{3,8,9,10,11,12} and Edward S. Boyden^{1,2,4,13,14,15,16} ✉

Expansion microscopy (ExM) physically magnifies biological specimens to enable nanoscale-resolution imaging using conventional microscopes. Current ExM methods permeate specimens with free-radical-chain-growth-polymerized polyacrylate hydrogels, whose network structure limits the local isotropy of expansion as well as the preservation of morphology and shape at the nanoscale. Here we report that ExM is possible using hydrogels that have a more homogeneous network structure, assembled via non-radical terminal linking of tetrahedral monomers. As with earlier forms of ExM, such 'tetra-gel'-embedded specimens can be iteratively expanded for greater physical magnification. Iterative tetra-gel expansion of herpes simplex virus type 1 (HSV-1) virions by ~10× in linear dimension results in a median spatial error of 9.2 nm for localizing the viral envelope layer, rather than 14.3 nm from earlier versions of ExM. Moreover, tetra-gel-based expansion better preserves the virion spherical shape. Thus, tetra-gels may support ExM with reduced spatial errors and improved local isotropy, pointing the way towards single-biomolecule accuracy ExM.

Expansion microscopy is in increasingly widespread use for biological imaging because it enables, via physical magnification of the specimen^{1–3}, nanoscale imaging on conventional, ubiquitous optical microscopes. In ExM, biological specimens are densely permeated by a swellable hydrogel. Biomolecules and/or fluorescent tags are covalently anchored to the hydrogel network, the specimen is chemically softened, and the hydrogel is expanded upon immersion in water (typically ~4.5× in linear dimension). Protocols using off-the-shelf-chemicals⁴ have helped ExM find utility in a wide variety of contexts, ranging from the mapping of ribosome components and RNAs in synaptic compartments⁵, to the analysis of circadian rhythm neural circuitry in the *Drosophila* brain⁶, to the analysis of cancer in human biopsies⁷. Variants of ExM have been developed that achieve nanoscale localization of proteins and RNAs in preserved cells and tissues on diffraction-limited microscopes^{4,7–13}. In addition, multiple strategies have been introduced to expand specimens ~10–20×, including applying the expansion process repeatedly (iterative expansion microscopy, or iExM)¹⁴ or by using superabsorbent hydrogels (X10 expansion microscopy)¹⁵. However, all ExM variants so far form the hydrogel mesh via free-radical chain-growth polymerization, a process that results in nanoscale structural heterogeneity in the hydrogel network^{16–20}. This raises the question of whether another polymer might provide better structural homogeneity, and thus less spatial error, during the expansion process.

To provide context we describe two earlier ExM protocols. One popular version of ExM is protein-retention expansion

microscopy (proExM)⁸. First, fixed biological specimens labelled with fluorophore-conjugated antibodies are exposed to a small molecule (acryloyl-X, SE, the succinimidyl ester of 6-((acryloyl) amino)hexanoic acid) that attaches a polymerizable acryloyl group to primary amine groups on antibodies and endogenous proteins. The specimen is then immersed in a solution containing sodium acrylate and acrylamide, as well as the cross-linker *N,N'*-methylenebisacrylamide, to form a dense network of cross-linked sodium polyacrylate/polyacrylamide hydrogel (PAAG) throughout the specimen. During the polymerization, antibodies and proteins are covalently anchored to the hydrogel via acryloyl-X, SE. Finally, proteinase K treatment cleaves most of the proteins, largely sparing the antibody-conjugated fluorophores, allowing expansion of the polymer-specimen composite in water. As a second example, in iExM¹⁴, fixed specimens are labelled first with primary antibodies and then with DNA oligonucleotide-conjugated secondary antibodies. Next, DNA oligonucleotides bearing a gel-anchorable moiety are hybridized to the secondary antibody-conjugated DNA oligonucleotides. Then a first hydrogel is formed as above, which anchors the gel-anchorable DNA oligonucleotides to the hydrogel at the locations of the immunostained proteins; this gel is made with a cleavable cross-linker. Subsequently, this gel is expanded as described above. Next, another round of hybridization of DNA oligonucleotides that are complementary to those anchored to the first hydrogel, and again bearing a gel-anchorable moiety, is performed. Then, a second hydrogel is formed throughout the expanded first

¹McGovern Institute for Brain Research, MIT, Cambridge, MA, USA. ²Media Arts and Sciences, MIT, Cambridge, MA, USA. ³Janelia Research Campus, Howard Hughes Medical Institute, Ashburn, VA, USA. ⁴Department of Biological Engineering, MIT, Cambridge, MA, USA. ⁵Broad Institute, MIT, Cambridge, MA, USA. ⁶Department of Neurology, Massachusetts General Hospital, Cambridge, MA, USA. ⁷Department of Microbiology and Physiological Systems, University of Massachusetts Medical School, Worcester, MA, USA. ⁸Department of Cell Biology, Harvard Medical School, Boston, MA, USA. ⁹Program in Cellular and Molecular Medicine, Boston Children's Hospital, Boston, MA, USA. ¹⁰Department of Pediatrics, Harvard Medical School, Boston, MA, USA. ¹¹Advanced Bioimaging Center, University of California at Berkeley, Berkeley, CA, USA. ¹²Department of Molecular and Cell Biology, University of California at Berkeley, Berkeley, CA, USA. ¹³MIT Center for Neurobiological Engineering, MIT, Cambridge, MA, USA. ¹⁴Department of Brain and Cognitive Sciences, MIT, Cambridge, MA, USA. ¹⁵Koch Institute, MIT, Cambridge, MA, USA. ¹⁶Howard Hughes Medical Institute, Cambridge, MA, USA. ¹⁷These authors contributed equally: Ruixuan Gao, Chih-Chieh (Jay) Yu. ✉e-mail: edboyden@mit.edu

hydrogel so that the new DNA oligonucleotides are anchored to the second hydrogel at the original sites of immunostained proteins. Finally, the first hydrogel is cleaved, allowing the second hydrogel to expand upon immersion in water. The protein locations can be imaged after the polymer-anchored oligonucleotides are labelled by applying complementary oligonucleotides, potentially equipped with branched DNA for amplification purposes, bearing fluorescent dyes. In short, the oligonucleotides provide a molecular mechanism (based on complementary strand hybridization) for signal transfer between the first and second hydrogels, as well as a scaffold for amplification and fluorescence readout.

In both cases, the free-radical chain-growth polymerization process that forms the PAAG has nanoscale structural heterogeneity. The size of local cross-linker density variations (Fig. 1a, '1') can amount to 15–25 nm for thus-synthesized polyacrylamide gels¹⁶. Topological defects, such as dangling ends (Fig. 1a, '2') and loops (Fig. 1a, '3'), can introduce deviations from uniform polymer meshes at the 1–10 nm length scale^{19,20}. So far, many attempts have been made to obtain a more ideal hydrogel matrix^{19–24}. One strategy has been to adopt step-growth polymerization. For example, photoinitiated thiol-ene step-growth polymerization formed a more homogeneous network structure versus that yielded by chain-growth polymerization^{25–27}. In another strategy, terminal linking of two kinds of tetrahedral poly(ethylene glycol) (PEG) monomer has been utilized to form a diamond lattice-like polymer network^{19,20,24}. The hydrogel thus formed, via non-radical step-growth polymerization, known as a tetra-PEG gel, approximates an ideal polymer network that is nearly void of structural defects, both as synthesized and when slightly swollen ($<1.5\times$ linear expansion in water)^{28,29}. The tetra-PEG gel structure has been further extended to create hydrogels with versatile chemical and mechanical properties, including polyelectrolyte hydrogels³⁰ and highly compressible and stretchable hydrogels³¹.

Here we report an ExM methodology using swellable hydrogels assembled by click-chemistry-based, non-radical linking of two complementary, tetrahedral monomers comprising backbones of polyacrylate and PEG respectively, which we call a tetra-gel (TG). TG-expanded herpes simplex virus type 1 (HSV-1) virions exhibited envelope shapes with substantially smaller spatial errors (9.2 nm of deviation) compared with classical PAAG-expanded virions (14.3 nm). As a result of these reduced spatial errors, TG-based ExM better preserves the spherical shapes of the virions compared with PAAG-based ExM. Thus, the TG serves as a candidate for a more structurally homogeneous ExM matrix compared with that synthesized by free-radical chain-growth polymerization, and points towards new ways of improving and extending the ExM toolbox.

Design of the TG structure and assembly mechanism

We designed and synthesized tetrahedral monomers closely related to those used for tetra-PEG gels (Fig. 1b)^{24,28–30}. One monomer (**1**) has a tetra-arm polyacrylate backbone with a clickable terminal azide group (synthesis and NMR spectra in Supplementary Figs. 1 and 2, respectively); the other monomer (**2**) has a tetra-arm PEG backbone with a complementary terminal alkyne group. The alkyne was varied to tune the reactivity of the terminal linking and functionality of the hydrogel (Fig. 1b, monomers **2'**, **2''** and **2'''**). The monomers have comparable molecular weights of ~10–20 kDa and an arm length of ~3–6 nm at the gelation step (at an ionic strength of ~0.150 M). In the solution phase, monomer **1** has four negatively charged polyacrylate arms ($n\approx 21$ acrylate units), each arm of which is estimated to extend ~4.0–5.7 nm, based on the previously characterized persistence length of ≥ 4.0 nm (ref. ³²) and the fully stretched length of ~5.7 nm. Monomer **2** has four uncharged PEG arms ($n\approx 57$ or $n\approx 114$ ethylene glycol units, depending on which version is used), each of which has a fully stretched length of ~21.7 or ~43.3 nm, respectively, which greatly exceeds its

persistence length of 0.38 nm³³. The PEG arm can thus be modelled as a freely jointed chain in solution^{34,35}, whose root-mean-square (r.m.s.) arm length can be calculated as ~2.9 or ~4.1 nm, respectively. For the synthesis of monomer **2**, the $n\approx 57$ backbone was used for variants **2'** and **2''** and the $n\approx 114$ backbone was used for variant **2'''**. The increased number of ethylene glycol units in **2'''** enhanced its solubility, compensating for the hydrophobic nature of the disulfide-dibenzocyclooctyne (SS-DBCO) moiety. Finally, when monomer **1** and a selected monomer **2** are mixed, a hydrogel forms via click-chemistry-based terminal linking (Fig. 1c, left). Then, in water or aqueous buffers with an ionic strength of $\lesssim 0.05$ M (the concentration estimated from Debye–Hückel theory for the electrostatic potential energy in electrolyte solutions)³⁶, the hydrogel swells due to the reduced electrostatic screening of salt ions between the mutually repelling monomer **1** units (~84 negative charges per monomer), which in turn elongates the originally unstructured PEG arms of the interconnecting monomer **2** (Fig. 1c, right).

Of the monomer **2** variants in Fig. 1b, the bicyclononyne (BCN) version (monomer **2''**) was designed to support the expansion of thicker specimens, because its slower click-reaction kinetics (by ~55% versus standard DBCO)³⁷ provide additional time for the monomers to equilibrate in concentration throughout the tissues during pre-gelation incubation. In addition, a slower gelation reaction³⁸ has been demonstrated to increase the homogeneity of the polymer network. Indeed, gelation occurs in ~1 and ~2.5 h at 4 °C for monomers **2'** and **2''**, respectively. The SS-DBCO version (monomer **2'''**) supports post-expansion cleavage of the polymer network into individual monomers, rendering it compatible with iterative expansion¹⁴. Monomer **2'''**-based gelation takes ~4 h at 4 °C, again suggesting its utility for thicker specimens.

TG expansion of cells and tissues

We mixed monomers **1** and **2** in a 1:1 ratio (although small deviations may occur depending on the exact fraction of monomer **1** whose *t*-butyl group was removed in the final step of its synthesis; Supplementary Fig. 1, bottom row); the gelling solution was then cast into a circular mould. Notably, deviation from a 1:1 ratio would result in additional defects in the polymer network and thus an increase in the structural heterogeneity²⁸. Using a virion-based local expansion isotropy assay (described later), we observed growing discrepancies versus the ground-truth virion size when the monomer ratio deviated from 1:1 (Supplementary Fig. 3). After 1–2 h of incubation at 37 °C, the gelling solution solidified into an optically transparent and mechanically elastic hydrogel (Fig. 2a, left). Similar to the PAAG gel and other types of hydrogel used in ExM that are formed by free-radical chain-growth polymerization^{7–13}, the gel swelled (approximately threefold in the linear dimension) after salt elution in water (Fig. 2a, right). Fluorescently labelled gels (Fig. 2b) showed the linear expansion factor to be ~3.0–3.5 \times .

Next, we implemented proExM using TG. We infused antibody-stained cells and tissue slices with NHS-azide (NHS = *N*-hydroxysuccinimide) to link proteins and antibodies (via primary amines) to the polymer network through click chemistry (Fig. 1b). We then formed the TG in situ, followed by the addition of proteinase K and swelling in water. In one implementation, HEK cells were immunostained with antibodies against microtubules and then processed using the DBCO version (monomer **2'**) of the TG. Water swelled the HEK cell–TG composite ~2.9-fold, resulting in more sharply resolved microtubules than could be seen before expansion using the same diffraction-limited confocal microscope (Fig. 2c). We aligned the pre- and post-expansion confocal microscopy images of the microtubules via non-rigid registration and quantified the amount of distortion in the expansion process (Fig. 2d), finding ~2.5% error over lengths of ~20 μ m, comparable to that of PAAG-based proExM^{1,8}. In another implementation, mouse brain slices expressing yellow fluorescent protein (YFP), processed

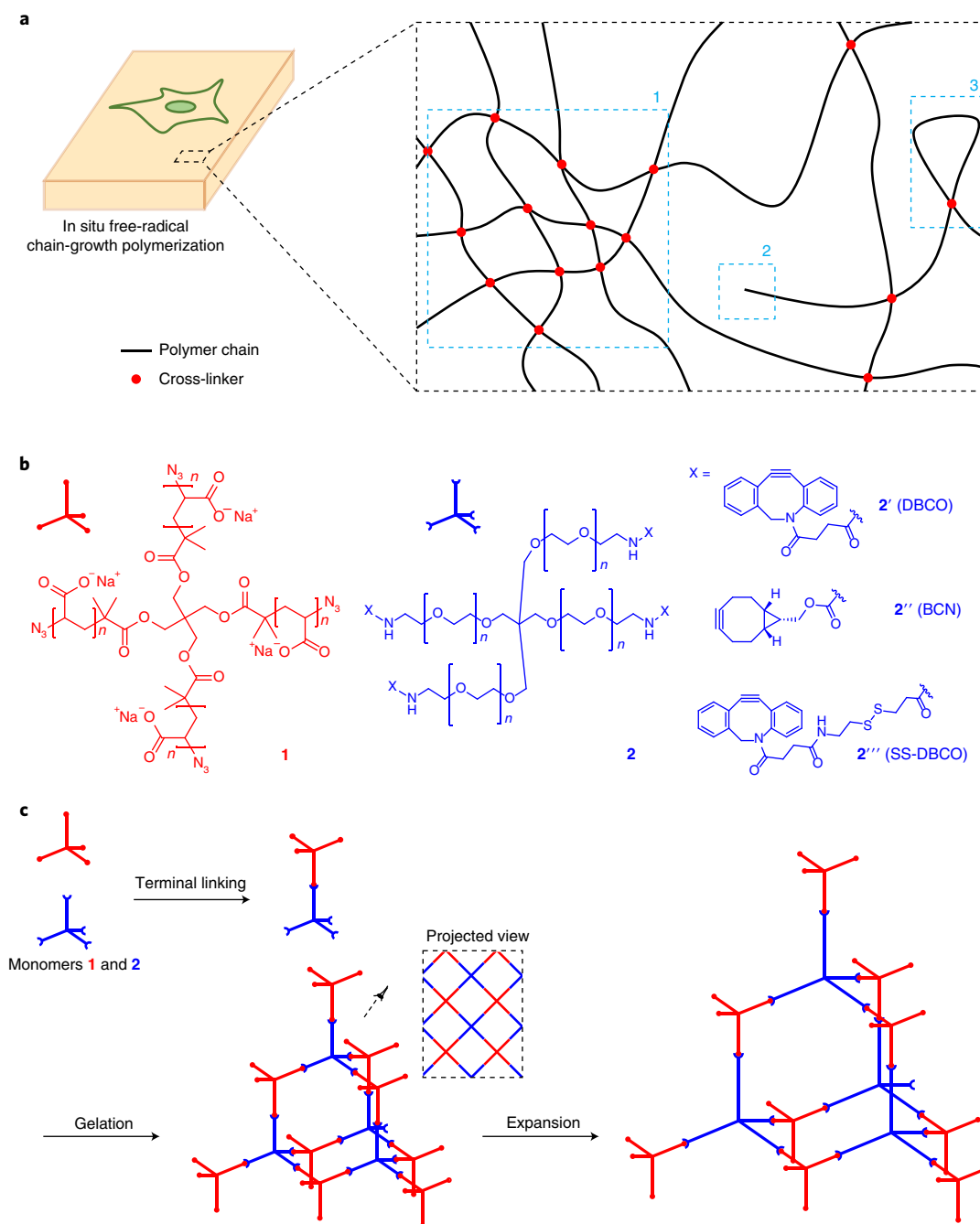


Fig. 1 | Design and synthesis of the tetra-gel (TG) for ExM. a, Cell/tissue–hydrogel composites formed by in situ free-radical chain-growth polymerization are known to have structural inhomogeneities in the range of tens of nanometres due to (1) local fluctuations of monomer and cross-linking densities, (2) dangling ends and (3) loops formed within the polymer network. **b**, Design of the TG monomers **1** and **2** with tetrahedral symmetry and reactive terminal groups. Specific monomer **2** terminal groups (**2'**, **2''** and **2'''**) enable, for example, control of the reaction rate between the monomers and the addition of functionalities to the polymer network. **c**, Formation and expansion of the TG via click-chemistry-based terminal linking of monomers **1** and **2**. Inset: projected view of the TG polymer network.

using the BCN version (monomer **2''**) of the TG, after immunostaining against YFP to enhance the fluorescence (Fig. 2e), expanded ~3.0-fold and showed excellent detail in structures such as dendritic spines, as seen with PAAG-based proExM⁸.

Since the TG is formed via non-radical polymerization, TG-based expansion could potentially preserve molecules that are inactivated during free-radical chain-growth polymerization. We found that the fluorescence of dyes known to be inactivated by PAAG-based proExM⁸ (Fig. 2f), including Alexa Fluor 647 (AF647), Cy5 and Alexa

Fluor 680 (AF680), was largely retained after TG-based expansion (Fig. 2f,g). Thus TG-based ExM may preserve molecules not compatible with PAAG-based ExM.

TG-based iterative expansion

The SS-DBCO version of the TG (using monomer **2'''**) would allow the TG polymer network to be cleaved at each network node (Fig. 3a), as appropriate for iExM¹⁴. Indeed, we found that HeLa cells, when expanded with TG, could be iteratively expanded (Fig. 3b).

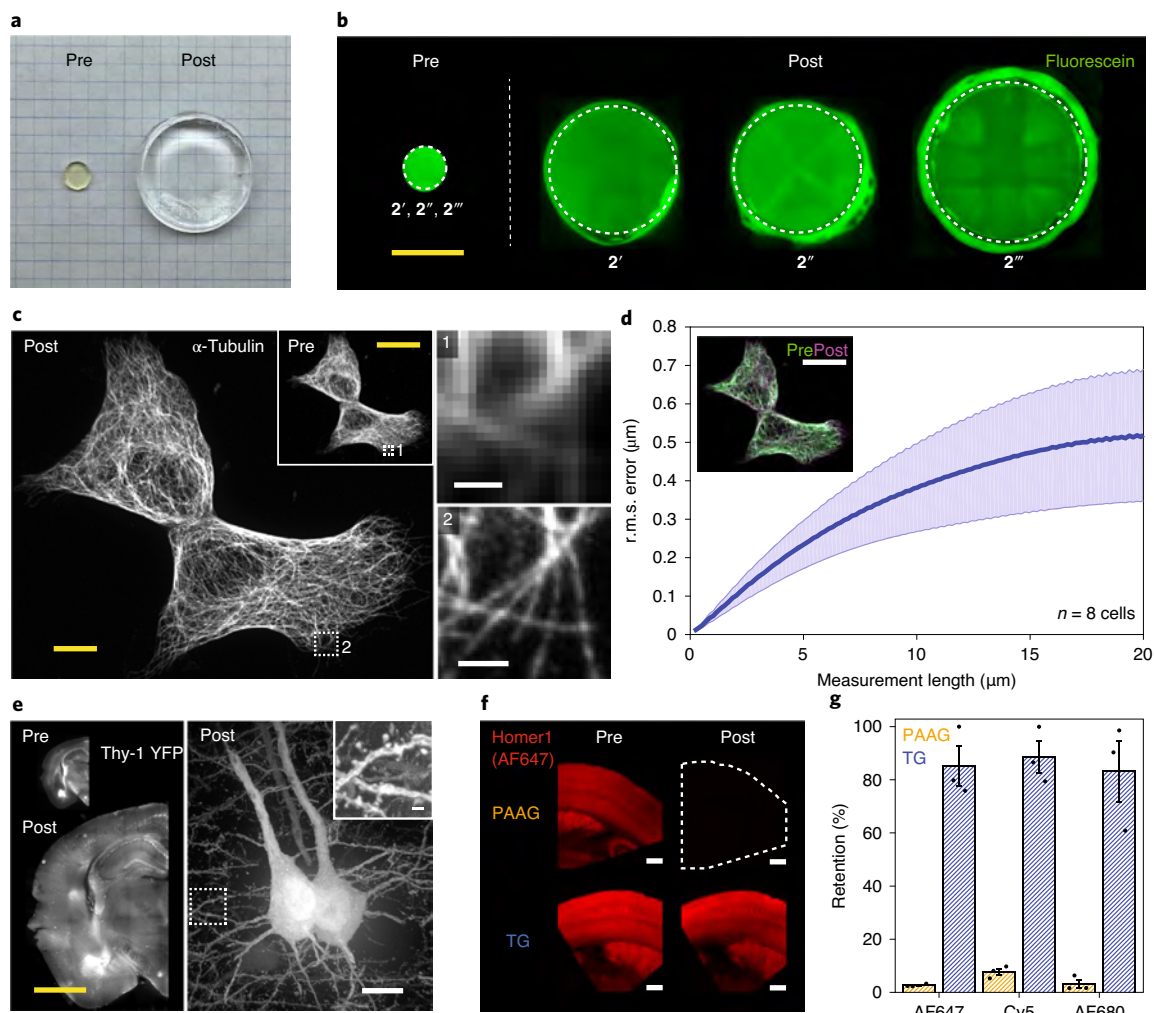


Fig. 2 | TG-mediated expansion of cells and tissues. **a**, Image of the TG (using monomer 2''') as synthesized (left, pre-expansion) and after swelling in deionized water (right, post-expansion). The two gels were cast in circular moulds with identical dimensions. Grid size, 5 mm. **b**, TG labelled with fluorescein in the pre-expansion state (left, 2'; the same sizes and shapes were obtained when 2'' and 2''' were used) and the post-expansion state (right, 2', 2'' and 2'''). Irregular boundaries on the post-expansion images reflect the meniscus of water used to expand the gels. Scale bar, 5 mm. **c**, Left, HEK293 cells with α -tubulin immunostaining in pre- (inset) and post-expansion states. Expansion factor, 2.85 \times . Scale bars, 20 μm . Right, magnified views of the boxed regions 1 (top) and 2 (bottom). Scale bars, 1 μm (2.85 μm). (Here and after, unless otherwise noted, the scale bar sizes are provided at the pre-expansion scale (that is, the biological scale) with the corresponding post-expansion size (that is, the physical size) indicated in parentheses.) Results are representative of five cells from the same cell culture. **d**, The r.m.s. error curve for HEK293 cell expansion (blue line, mean; shaded area, standard deviation; $n = 8$ cells from one culture). Inset: non-rigidly registered and overlaid pre- (green) and post-expansion (magenta) images used for the r.m.s. error analysis. Scale bar, 20 μm (57 μm). **e**, Pre- (left top) and post-expansion (left bottom and right) Thy1-YFP mouse brain slices. Expansion factor, 3.00 \times . Scale bars, 5 mm (left) and 10 μm (right, 30 μm). The gelled brain slice in the lower left panel was immunostained against yellow fluorescent protein (YFP) after the proteolysis step to enhance the fluorescence. Inset: magnified view of the boxed region. Scale bar, 1 μm (3 μm). Results are representative of two slices from the same single batch of brain slice preparation for each panel. **f**, Pre-expansion (left column) and post-expansion (right column) Thy1-YFP mouse brain slices immunostained with Homer1 primary antibody and AF647-conjugated secondary antibody, using PAAG (top row) and TG (bottom row). Expansion factor, 3.93 \times (PAAG) and 2.72 \times (TG). Scale bars, 300 μm (top right, 1.18 mm; bottom right, 815 μm). Results are representative of three slices from the same single batch of brain slice preparation for each gel type. **g**, Fluorescence retention of AF647, Cy5 and AF680 with PAAG and TG in immunostained mouse brain slices processed as in **f** (bar height, mean; black dots, individual data points; error bar, standard error of the mean; $n = 3$ brain slices from one mouse).

We used a free-radical-chain-growth-polymerized gel for the second round of iExM, reasoning that the spatial errors introduced by the second-round expansion would be negligible compared with those introduced by the first round (since, when considered in biological units, that is, in terms of the relative spacing of biomolecules with respect to each other, second-round errors are effectively divided by the expansion factor of the first round). TG-based iExM expanded the cells by approximately 16-fold, revealing the hollow structure of

the microtubules (Fig. 3c), with a sidewall separation comparable to that seen previously with iExM of BS-C-1 cells using PAAG-based iExM (Fig. 3d). We note that, compared with that observed, for example, by STORM (stochastic optical reconstruction microscopy), the larger sidewall distance seen here can be explained by the label size effect described previously—classical iExM requires larger labels than used in other super-resolution methods¹⁴. Finally, multiple DNA oligonucleotide-conjugated antibodies could be used at

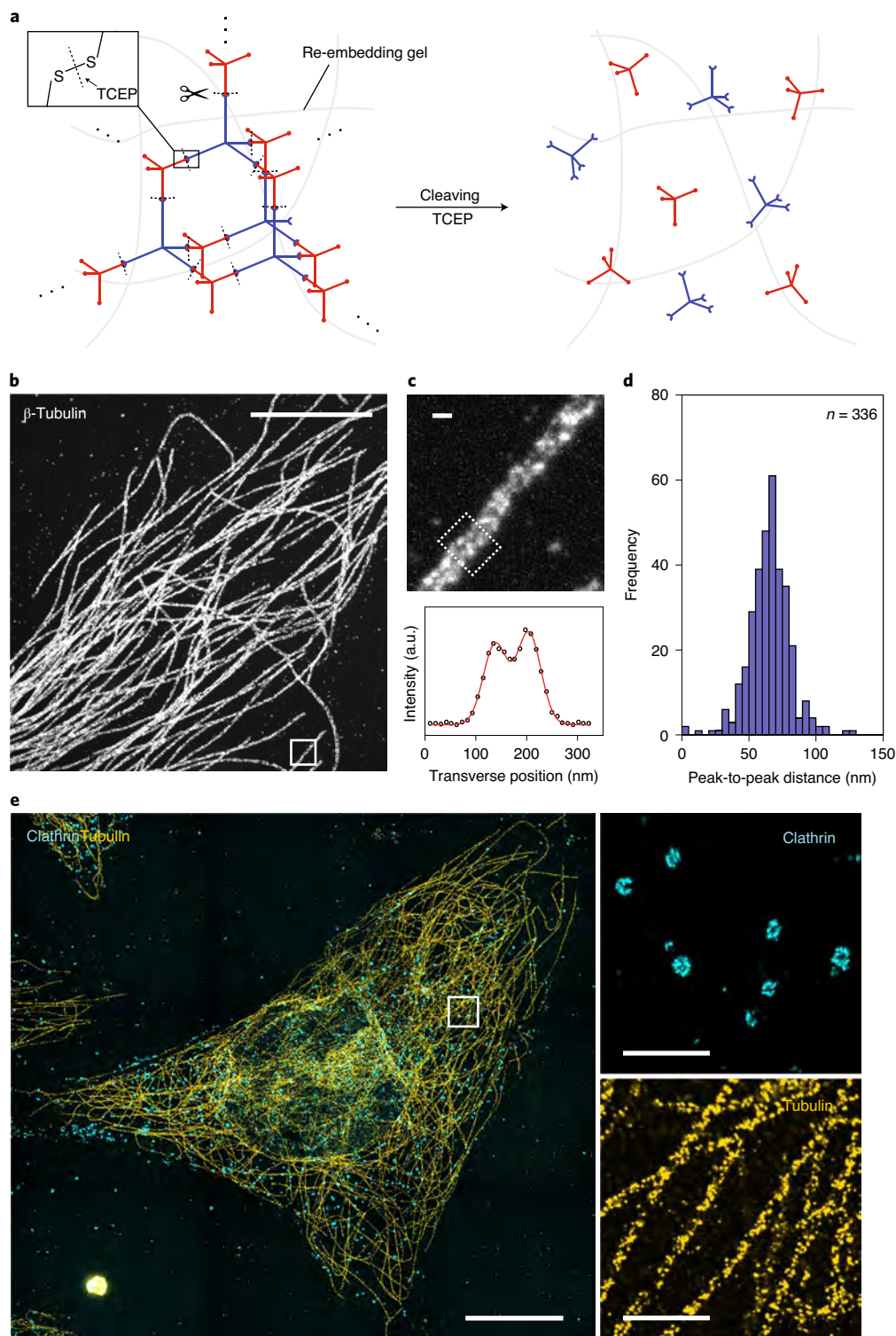


Fig. 3 | TG-based iterative expansion. **a**, Monomeric cleaving of TG (monomer **2''**) after re-embedding in a second hydrogel. A reducing agent, tris(2-carboxyethyl)phosphine (TCEP), was applied to cleave the disulfide bonds in the TG polymer network. **b**, HeLa cell with β -tubulin immunostaining, expanded by cleavable TG-based two-round iterative expansion. Expansion factor, 15.6 \times . Scale bar, 5 μm (78.2 μm). Results are representative of ten cells from the same cell culture. **c**, Top, magnified view of the boxed region in **b**. Scale bar, 100 nm (1.56 μm). Bottom, transverse line intensity profile of the microtubule in a single xy plane in the dashed box (circle points) and the fitted sum of two Gaussians (red line). The line intensity profile was averaged in the direction parallel to the microtubule axis over a length of 200 nm. **d**, Histogram of peak-to-peak distance between microtubule sidewalls in HeLa cells ($n = 336$ segments of a length of 200 nm from ten cells in one culture). **e**, Left, HeLa cell with two-colour labelling of clathrin-coated pits/vesicles and microtubules, expanded by TG-based two-round iterative expansion. Expansion factor, 15.6 \times . Scale bar, 10 μm (156 μm). Right, magnified view of the boxed region for each colour channel. Scale bars, 1 μm (15.6 μm). Results are from one cell from the same cell culture preparation as in **b**.

once, for example, to label tubulin and clathrin in the TG-expanded HeLa cells (Fig. 3e)¹⁴.

Spatial analysis of the TG-based ExM expansion error

To assess the spatial errors introduced by TG-based iExM, we imaged the nanoscale arrangement of virion envelope proteins. To minimize the label size effect mentioned above, we developed a direct, non-specific labelling strategy that targets primary amines of virus envelope proteins and reduces the label size from ~21 nm (ref. 14) to that of a single DNA oligonucleotide (~7 nm). First, we directly conjugated 22-base-pair oligonucleotides to the envelope proteins on the virions via a hydrazone-based DNA-to-peptide conjugation (Fig. 4a). We were careful not to expose viruses to any buffers containing detergents, for all steps from fixation to gelation, aiming to preserve the integrity of the virion's lipid bilayer envelope and directing the majority of the labelling to accessible envelope proteins on the outside of the membrane. HSV-1 virions have a well-defined envelope protein layer that has been characterized by methods such as electron microscopy^{39–41}, electron tomography^{42,43} and super-resolution microscopy⁴⁴, and they have an appropriate length scale (170–190 nm diameter)⁴⁴, with features in the tens of nanometres, for characterizing the local homogeneity of the TG. After direct labelling of the envelope proteins, we then expanded the HSV-1 virions with TG-based iExM versus PAAG-based iExM (in both cases using PAAGs in the second round; Fig. 4b). We noted that this protocol was compatible with dual-colour labelling and imaging of envelope proteins and DNA (Supplementary Fig. 4) and could be applied to other types of enveloped viruses, such as the vesicular stomatitis virus (VSV), which is an RNA virus (Supplementary Fig. 5), and the human immunodeficiency virus (HIV), which is a retrovirus (Supplementary Fig. 6). For the quantitative analysis of envelope shapes, to gauge the TG-based iExM spatial error, we focused on viruses that have a spherical geometry (that is, HSV-1^{42,43} and HIV⁴⁵).

The expansion factor for TG-based iExM of the HSV-1 virions was ~10.3–13.3, and for PAAG-based iExM it was ~15.3–18.7. TG-based iExM appeared to result in more spherical virions than PAAG-based iExM (Fig. 4c). From single-particle averaged virion images, we found that the envelope protein profile of the TG-expanded HSV-1 virions was substantially sharper than that for the PAAG-expanded virions (Fig. 4d). Similarly, the TG-expanded

HIV virions had sharper envelope profiles than the PAAG-expanded ones (Fig. 4e).

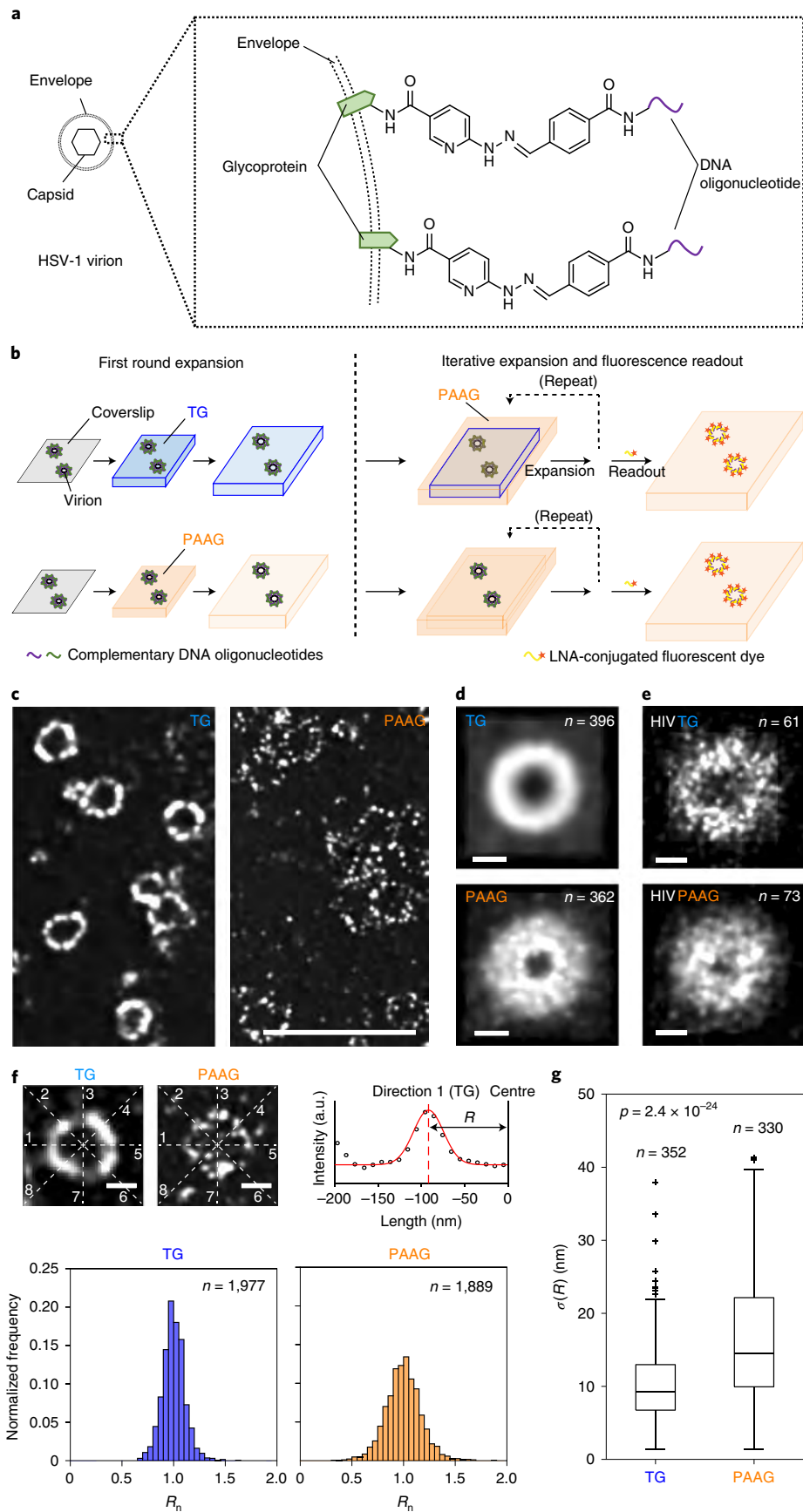
To quantify the spatial errors associated with each expansion process, we measured the standard deviation of the virion radius (σ) within the midplane of individual HSV-1 virions (Fig. 4f; computed in biological units, that is, normalized by the expansion factor, to compensate for the different expansion factors of the TG- and PAAG-based iExM protocols). The TG-expanded HSV-1 virions [σ_m (median σ across virions) = 9.2 nm; $n = 352$ virions; virions from a single batch of live HSV-1 preparation] had a significantly smaller σ_m value compared with the PAAG-expanded HSV-1 virions ($\sigma_m = 14.3$ nm; $n = 330$ virions; virions from the same single batch of live HSV-1 preparation; $p = 2.4 \times 10^{-24}$, two-sided Wilcoxon rank sum test; Fig. 4g). We calculated the same metric of σ for the single-particle averaged images of the HSV-1 virions (Fig. 4d) and saw smaller spatial errors for the TG-expanded virions [σ_a (σ of the averaged virion image) = 3.4 nm] compared with the PAAG-expanded ones ($\sigma_a = 4.0$ nm); note that the absolute difference between the two σ_a values was numerically small because of population averaging. HIV virions have much sparser envelope proteins per virion than HSV-1 virions, which precludes computing σ at the individual particle level; however, for single-particle averaged images, the TG-expanded HIV virions ($\sigma_a = 8.9$ nm) had a smaller σ_a value than the PAAG-expanded ones ($\sigma_a = 12.9$ nm), showing again the reduced spatial errors for TG-based iExM (Fig. 4e).

We made a unifying computational model so that different measures of hydrogel-based variability could be compared. We took the spatial errors calculated across individual particles (Fig. 4g) as the gold-standard metrics of spatial error, and sought to examine whether or not other metrics, such as those derived from single-particle averaged images (Fig. 4d,e), were consistent. For the model, we considered both chemical variability (for example, the hydrogel-associated local anisotropy) and biological variability (for example, the biological distribution of virion size). We developed a computational model that simulated the averaged images from individual simulated virions (Supplementary Methods and Supplementary Fig. 7). When single-particle averaged images were simulated based on this model, we observed sharper envelope profiles for TG than PAAG, consistent with the experimental results (Supplementary Fig. 7). Moreover, the metrics derived from the

Fig. 4 | Spatial errors introduced by TG-based versus classical PAAG-based iterative expansion. **a**, Short DNA oligonucleotides (22 base pairs) were covalently conjugated to the envelope proteins of HSV-1 virions via hydrazone formation, which allows labelling transfer across multiple hydrogels, amplification based on branched DNA, and fluorescence readout based on the hybridization of fluorescent oligonucleotides. **b**, Schematic illustration of TG- (top) and PAAG-based (bottom) iterative expansion of HSV-1 virions with the direct oligonucleotide-conjugation as in **a**. PAAG-based re-embedding and expansion was used for all expansion rounds after the first round, based on the reasoning that most of the error of an iterative expansion protocol is introduced in the first round of expansion (see text for details). **c**, HSV-1 virions with directly labelled envelope proteins, expanded by TG- (left) and PAAG-based (right) two-round iterative expansion. Scale bar (for both panels), 1 μm (TG, 10.3 μm ; PAAG, 15.3 μm). Expansion factor, 10.3 \times (TG) and 15.3 \times (PAAG). Results are representative of three separately acquired fields of view from a single hydrogel preparation for each gel type, using virions from the same single batch of live HSV-1 preparation. **d**, Single-particle averaged images of HSV-1 virions after TG (top)- and PAAG-based (bottom) two-round iterative expansion (TG, $n = 396$; PAAG, $n = 362$ virions; virions from the same single batch of live HSV-1 preparation). Full width half maximum measurements of the radial intensity profile (the line intensity profile from the particle centre to the edge of the particle), 73.6 nm (TG) and 91.0 nm (PAAG). Scale bars, 100 nm. **e**, Single-particle averaged images of HIV virions expanded by TG- (top) and PAAG-based (bottom) two-round iterative expansion (TG, $n = 61$; PAAG, $n = 73$ virions; virions from the same single batch of live HIV preparation). Full width half maximum measurements of the radial intensity profile, 49.1 nm (TG) and 119.0 nm (PAAG). Scale bars, 100 nm. **f**, Top left and middle, representative single xy -plane images of HSV-1 virions expanded by TG- and PAAG-based two-round iterative expansion. White dashed lines indicate the eight directions along which the virion radius (R) was measured. Scale bars, 100 nm. Top right, representative line intensity profile (circle points) along a single direction (Direction 1) of the TG-expanded virion and the fitted Gaussian (red line). The distance from the centre of the Gaussian to the centre of the virion was defined as R along that direction. Bottom, histograms of the particle-mean-normalized R (R_n) for all measured line profiles [TG, $n = 1,977$; PAAG, $n = 1,889$ profiles; from 352 (TG) and 330 (PAAG) virions from the same single batch of live HSV-1 preparation]. **g**, Standard deviation (σ) of HSV-1 virion radius (R) within individual virions for TG- and PAAG-based iterative expansion ($p = 2.4 \times 10^{-24}$, two-sided Wilcoxon rank sum test; TG, $n = 352$; PAAG, $n = 330$ virions; virions from the same single batch of live HSV-1 preparation). Data are presented as box plots, where the ends of the whiskers represent the maximum and minimum values of the distribution after outlying points (values above the 75th percentile + 1.5 \times interquartile range, or below the 25th percentile - 1.5 \times interquartile range) have been excluded, and where the upper line of the box represents the 75th percentile, the middle line represents the 50th percentile (median), the lower line represents the 25th percentile and the plus signs represent the individual values of the outlying points.

simulated images were comparable to the experimental values to a great extent, despite the highly simplified assumptions and designs of the model.

To assess how the improved accuracy of TG- versus PAAG-based expansion helps to preserve the shapes of nanoscale objects like viruses, we characterized the expanded HSV-1 virion



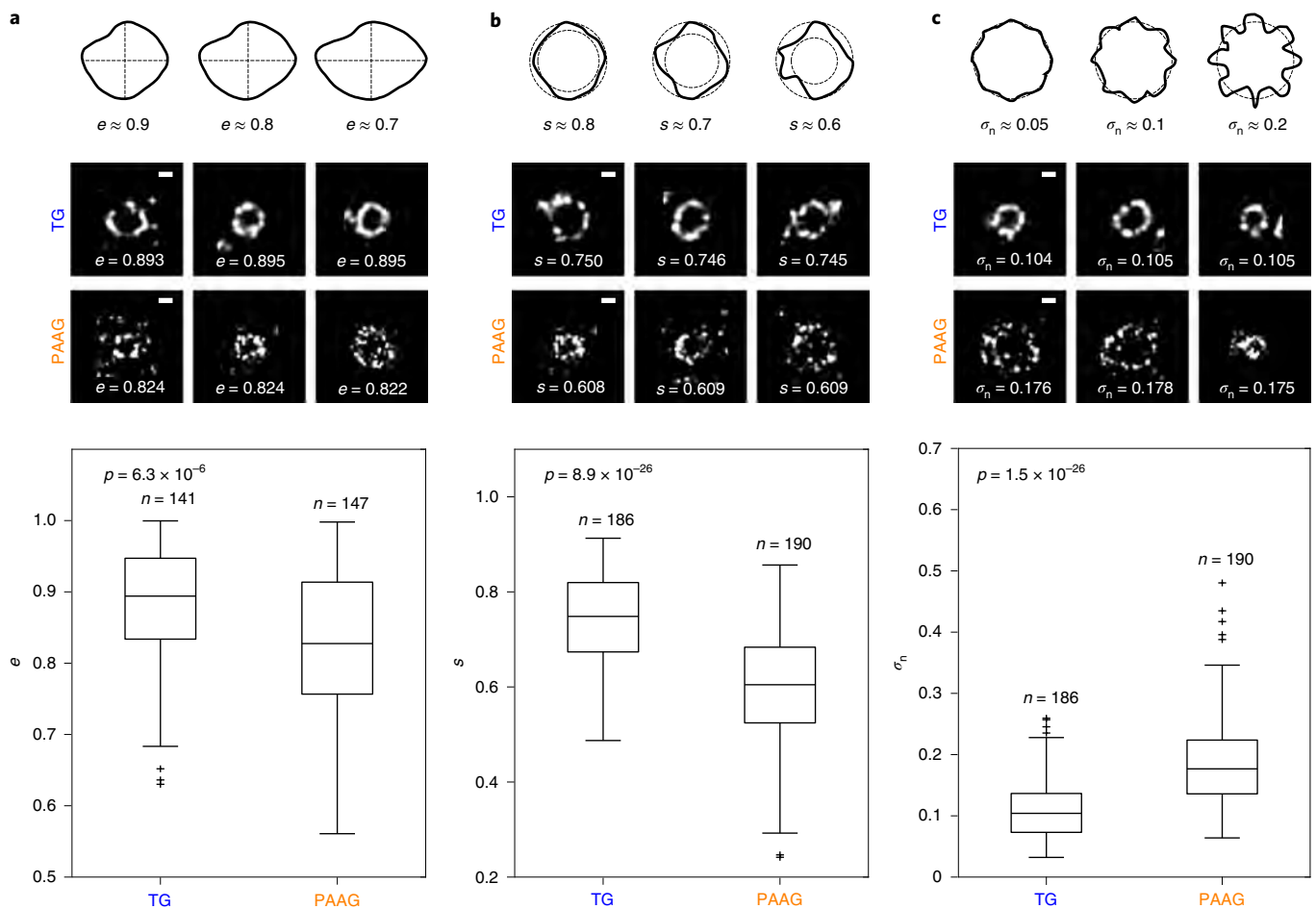


Fig. 5 | Shape analysis of TG- versus PAAG-expanded HSV-1 virions. a, Top, schematic examples of shapes with eccentricity (e) values of ≈ 0.9 , 0.8 and 0.7 . Middle, HSV-1 virions expanded by TG- (top row) and PAAG-based (bottom row) two-round iterative expansion, with the z-midplane cross-sectional shapes scoring close to the median value of e within each hydrogel group. Scale bars, 100 nm. Bottom, eccentricity values of HSV-1 virion z-midplane cross-sections for TG- and PAAG-based iterative expansion ($p = 6.3 \times 10^{-6}$, two-sided Wilcoxon rank sum test; TG, $n = 141$; PAAG, $n = 147$ virions; virions from the same single batch of live HSV-1 preparation). **b**, Top, schematic examples of shapes with sphericity (s) values of ≈ 0.8 , 0.7 and 0.6 . Middle, HSV-1 virions expanded by TG- (top row) and PAAG-based (bottom row) two-round iterative expansion, with the z-midplane cross-sectional shapes scoring close to the median value of s within each hydrogel group. Scale bars, 100 nm. Bottom, sphericity values of HSV-1 virion z-midplane cross-sections for TG- and PAAG-based iterative expansion ($p = 8.9 \times 10^{-26}$, two-sided Wilcoxon rank sum test; TG, $n = 186$; PAAG, $n = 190$ virions; virions from the same single batch of live HSV-1 preparation). **c**, Top, schematic examples of shapes with normalized circular standard deviation (σ_n) values of ≈ 0.05 , 0.1 and 0.2 . Middle, HSV-1 virions expanded by TG- (top row) and PAAG-based (bottom row) two-round iterative expansion, with the z-midplane cross-sectional shapes scoring close to the median value of σ_n within each hydrogel group. Scale bars, 100 nm. Bottom, normalized circular standard deviation values of HSV-1 virion z-midplane cross-sections for TG- and PAAG-based iterative expansion ($p = 1.5 \times 10^{-26}$, two-sided Wilcoxon rank sum test; TG, $n = 186$; PAAG, $n = 190$ virions; virions from the same single batch of live HSV-1 preparation). In **a–c**, data are presented as box plots, where the ends of the whiskers represent the maximum and minimum values of the distribution after outlying points (values above the 75th percentile $+ 1.5 \times$ interquartile range, or below the 25th percentile $- 1.5 \times$ interquartile range) have been excluded, and where the upper line of the box represents the 75th percentile, the middle line represents the 50th percentile (median), the lower line represents the 25th percentile and the plus signs represent the individual values of the outlying points.

cross-sectional shapes using key shape descriptors, such as the eccentricity (e), the ratio of the minor axis to the major axis ($e = 1$ for a perfect circle; see the upper sketches in Fig. 5a for examples of shapes with different e values), the sphericity (s), the ratio of the radius of the inscribing circle to the radius of the circumscribing circle ($s = 1$ for a perfect circle; see the upper sketches in Fig. 5b for examples of shapes with different s values), and the normalized circular standard deviation (σ_n), the standard deviation of the eight radii within each particle divided by the mean for that particle ($\sigma_n = 0$ for a perfect circle; see the upper sketches in Fig. 5c for examples of shapes with different σ_n values). We found that the TG-expanded virions were significantly closer to circular compared

with the PAAG-expanded virions ($p < 10^{-5}$ for all the descriptors, two-sided Wilcoxon rank sum test; Fig. 5). The changes were not small: the median deviation from a perfect circle was substantially reduced for TG compared with PAAG, by 62% (e), 64% (s) and 59% (σ_n) of the PAAG deviation. We applied the same shape analysis to the HIV virions and obtained data consistent with the HSV-1 values (Supplementary Fig. 6). In the future, even higher expansion factors, potentially revealing individual proteins on the virions, may be possible by expanding $\sim 40\times$ via three rounds of iterative expansion, with the initial expansion round being TG-based and the final two rounds being PAAG-based (Supplementary Fig. 8 and Supplementary Video 1).

Conclusions

We have found that TG polymers, assembled via non-radical step-growth polymerization of tetrahedral monomers, are capable of mediating ExM. When TG-based iterative expansion protocols were compared with classical PAAG-based protocols, using HSV-1 virion envelope proteins as the assay, we saw a reduction in spatial errors introduced by the expansion process, from 14.3 to 9.2 nm at the individual particle level. Using multiple classical shape descriptors such as ellipticity and sphericity to capture the improvements of TG over PAAG, we also found that TG-based iExM better retained the nanoscale shape of the HSV-1 virion envelope. Thus, TG-based ExM may overcome the local anisotropy of the expansion process that is inherent in previously used methods, and it may enable expansion with better preserved nanoscale morphology and shape. The single-digit distortions introduced by TG-based ExM raise the tantalizing question of whether new hydrogel chemistries may be able to achieve expansion accuracy approaching that of the size of individual biomolecules such as proteins.

Our current study is focused on the design principles of the hydrogel matrices for ExM, and it is not yet a protocol for general scientific use. For TG-based ExM to be useful in everyday scientific investigations, a number of improvements will be required. The chemicals must be made broadly available, through commercialization or other arrangements. Biomolecules of interest are currently anchored to the ends of monomers when incorporated into the hydrogel network, meaning that every anchored biomolecule results in a 'defect' in the polymer network because it terminates one of the monomer's arms; replacing such terminal-based anchoring with sidechain-based anchoring may improve TG structural homogeneity for ExM further. The ideal size of the monomer has not yet been established: current TG-based ExM monomers are much larger than the sodium acrylate monomers used in classical ExM protocols, raising the question of whether smaller TG monomers would better permeate dense cells and tissues. Finally, appreciation of the improvements offered by TG over PAAG will most likely require post-expansion antibody staining, or the use of very small tags such as nanobodies for pre-expansion staining, since the improvements offered by TG are smaller than the sizes of antibodies. To enable post-expansion antibody staining, the disulfide in the monomer will need to be replaced by a cleavable moiety that is compatible with the high-temperature treatments, basic pH environments and other conditions typically used to denature proteins and expand them away from each other^{4,8,11}. For this approach, intramolecular epoxide cross-linking might be helpful for epitope preservation⁴⁶. In the future, such a second-generation TG-based ExM process may be useful for investigating the detailed nanoscale spatial arrangement of molecular species in complexes, in cells and tissues, and in healthy and disease states.

Online content

Any methods, additional references, Nature Research reporting summaries, source data, extended data, supplementary information, acknowledgements, peer review information; details of author contributions and competing interests; and statements of data and code availability are available at <https://doi.org/10.1038/s41565-021-00875-7>.

Received: 18 November 2019; Accepted: 11 February 2021;
Published online: 29 March 2021

References

- Chen, F., Tillberg, P. W. & Boyden, E. S. Expansion microscopy. *Science* **347**, 543–548 (2015).
- Gao, R., Asano, S. M. & Boyden, E. S. Q&A: expansion microscopy. *BMC Biol.* **15**, 50 (2017).
- Wassie, A. T., Zhao, Y. & Boyden, E. S. Expansion microscopy: principles and uses in biological research. *Nat. Methods* **16**, 33–41 (2019).
- Asano, S. M. et al. Expansion microscopy: protocols for imaging proteins and RNA in cells and tissues. *Curr. Protoc. Cell Biol.* **80**, e56 (2018).
- Hafner, A. S., Donlin-Asp, P. G., Leitch, B., Herzog, E. & Schuman, E. M. Local protein synthesis is a ubiquitous feature of neuronal pre- and postsynaptic compartments. *Science* **364**, eaau3644 (2019).
- Schlichting, M. et al. Light-mediated circuit switching in the *Drosophila* neuronal clock network. *Curr. Biol.* **29**, 3266–3276.e3 (2019).
- Zhao, Y. et al. Nanoscale imaging of clinical specimens using pathology-optimized expansion microscopy. *Nat. Biotechnol.* **35**, 757–764 (2017).
- Tillberg, P. W. et al. Protein-retention expansion microscopy of cells and tissues labeled using standard fluorescent proteins and antibodies. *Nat. Biotechnol.* **34**, 987–992 (2016).
- Chozinski, T. J. et al. Expansion microscopy with conventional antibodies and fluorescent proteins. *Nat. Methods* **13**, 485–488 (2016).
- Chen, F. et al. Nanoscale imaging of RNA with expansion microscopy. *Nat. Methods* **13**, 679–684 (2016).
- Ku, T. et al. Multiplexed and scalable super-resolution imaging of three-dimensional protein localization in size-adjustable tissues. *Nat. Biotechnol.* **34**, 973–981 (2016).
- Gambarotto, D. et al. Imaging cellular ultrastructures using expansion microscopy (U-ExM). *Nat. Methods* **16**, 71–74 (2019).
- Gao, R. et al. Cortical column and whole-brain imaging with molecular contrast and nanoscale resolution. *Science* **363**, eaau8302 (2019).
- Chang, J.-B. et al. Iterative expansion microscopy. *Nat. Methods* **14**, 593–599 (2017).
- Truckenbrodt, S. et al. X10 expansion microscopy enables 25 nm resolution on conventional microscopes. *EMBO Rep.* **19**, e45836 (2018).
- Cohen, Y., Ramon, O., Kopelman, I. J. & Mizrahi, S. Characterization of inhomogeneous polyacrylamide hydrogels. *J. Polym. Sci. B Polym. Phys.* **30**, 1055–1067 (1992).
- Yazici, I. & Okay, O. Spatial inhomogeneity in poly(acrylic acid) hydrogels. *Polymer* **46**, 2595–2602 (2005).
- Orakdogan, N. & Okay, O. Correlation between crosslinking efficiency and spatial inhomogeneity in poly(acrylamide) hydrogels. *Polym. Bull.* **57**, 631–641 (2006).
- Di Lorenzo, F. & Seiffert, S. Nanostructural heterogeneity in polymer networks and gels. *Polym. Chem.* **6**, 5515–5528 (2015).
- Gu, Y., Zhao, J. & Johnson, J. A. A (macro)molecular-level understanding of polymer network topology. *Trends Chem.* **1**, 318–334 (2019).
- Martens, P. & Anseth, K. S. Characterization of hydrogels formed from acrylate modified poly(vinyl alcohol) macromers. *Polymer* **41**, 7715–7722 (2000).
- Lutolf, M. P. & Hubbell, J. A. Synthesis and physicochemical characterization of end-linked poly(ethylene glycol)-co-peptide hydrogels formed by Michael-type addition. *Biomacromolecules* **4**, 713–722 (2003).
- Malkoch, M. et al. Synthesis of well-defined hydrogel networks using Click chemistry. *Chem. Commun.* 2774–2776 (2006).
- Sakai, T. et al. Design and fabrication of a high-strength hydrogel with ideally homogeneous network structure from tetrahedron-like macromonomers. *Macromolecules* **41**, 5379–5384 (2008).
- Fairbanks, B. D. et al. A versatile synthetic extracellular matrix mimic via thiol-norbornene photopolymerization. *Adv. Mater.* **21**, 5005–5010 (2009).
- Cui, J. et al. Synthetically simple, highly resilient hydrogels. *Biomacromolecules* **13**, 584–588 (2012).
- Saffer, E. M. et al. SANS study of highly resilient poly(ethylene glycol) hydrogels. *Soft Matter* **10**, 1905–1916 (2014).
- Matsunaga, T., Sakai, T., Akagi, Y., Chung, U.-i. & Shibayama, M. Structure characterization of Tetra-PEG gel by small-angle neutron scattering. *Macromolecules* **42**, 1344–1351 (2009).
- Matsunaga, T., Sakai, T., Akagi, Y., Chung, U.-i. & Shibayama, M. SANS and SLS studies on tetra-arm PEG gels in as-prepared and swollen states. *Macromolecules* **42**, 6245–6252 (2009).
- Oshima, K., Fujimoto, T., Minami, E. & Mitsukami, Y. Model polyelectrolyte gels synthesized by end-linking of tetra-arm polymers with click chemistry: synthesis and mechanical properties. *Macromolecules* **47**, 7573–7580 (2014).
- Kamata, H., Akagi, Y., Kayasuga-Kariya, Y., Chung, U.-i. & Sakai, T. "Nonswellable" hydrogel without mechanical hysteresis. *Science* **343**, 873–875 (2014).
- Tricot, M. Comparison of experimental and theoretical persistence length of some polyelectrolytes at various ionic strengths. *Macromolecules* **17**, 1698–1704 (1984).
- Kienberger, F. et al. Static and dynamical properties of single poly(ethylene glycol) molecules investigated by force spectroscopy. *Single Mol.* **1**, 123–128 (2000).
- Kuhn, W. Über die Gestalt fadenförmiger Moleküle in Lösungen. *Kolloid Z.* **68**, 2–15 (1934).
- Kuhn, W. & Kuhn, H. Die Frage nach der Aufrollung von Fadenmolekeln in strömenden Lösungen. *Helv. Chim. Acta* **26**, 1394–1465 (1943).

36. Debye, P. & Hückel, E. The theory of electrolytes. I. Lowering of freezing point and related phenomena. *Phys. Z.* **24**, 185–206 (1923).
37. Dommerholt, J., Rutjes, F. P. J. T. & van Delft, F. L. Strain-promoted 1,3-dipolar cycloaddition of cycloalkynes and organic azides. *Top. Curr. Chem.* **374**, 16 (2016).
38. Zander, Z. K., Hua, G., Wiener, C. G., Vogt, B. D. & Becker, M. L. Control of mesh size and modulus by kinetically dependent cross-linking in hydrogels. *Adv. Mater.* **27**, 6283–6288 (2015).
39. Hughes, M. P., Morgan, H. & Rixon, F. J. Dielectrophoretic manipulation and characterization of herpes simplex virus-1 capsids. *Eur. Biophys. J.* **30**, 268–272 (2001).
40. Liu, F. & Zhou, Z. H. in *Human Herpesviruses: Biology, Therapy, and Immunoprophylaxis* (eds Arvin, A. et al.) 27–43 (Cambridge Univ. Press, 2007).
41. Brown, J. C. & Newcomb, W. W. Herpesvirus capsid assembly: Insights from structural analysis. *Curr. Opin. Virol.* **1**, 142–149 (2011).
42. Grünewald, K. et al. Three-dimensional structure of herpes simplex virus from cryo-electron tomography. *Science* **302**, 1396–1398 (2003).
43. Maurer, U. E., Sodeik, B. & Grünewald, K. Native 3D intermediates of membrane fusion in herpes simplex virus 1 entry. *Proc. Natl Acad. Sci. USA* **105**, 10559–10564 (2008).
44. Laine, R. F. et al. Structural analysis of herpes simplex virus by optical super-resolution imaging. *Nat. Commun.* **6**, 5980 (2015).
45. Liu, J., Wright, E. R. & Winkler, H. in *Cryo-EM, Part C: Analyses, Interpretation, and Case studies* Vol. 483 (ed. Jensen, G. J.) 267–290 (Academic, 2010).
46. Park, Y.-G. et al. Protection of tissue physicochemical properties using polyfunctional crosslinkers. *Nat. Biotechnol.* **37**, 73–83 (2019).

Publisher's note Springer Nature remains neutral with regard to jurisdictional claims in published maps and institutional affiliations.

© The Author(s), under exclusive licence to Springer Nature Limited 2021

Methods

Synthesis of TG monomers. Monomer 1 was synthesized using a procedure modified from a previously described synthesis (Supplementary Fig. 1)³⁰. First, tetra-arm poly(*t*-butyl acrylate) with bromo terminal groups (4) was synthesized by atom transfer radical polymerization. Next, tetra-arm poly(*t*-butyl acrylate) with azide terminal groups (5) was synthesized by replacing the bromo groups of 4 with azides (Supplementary Fig. 2). Finally, monomer 1 was synthesized by hydrolysis and neutralization of 5 to a final pH \approx 7. Monomers 2', 2'' and 2''' were synthesized by NHS ester-based conjugation of the alkynes (DBCO-NHS, BCN-NHS or DBCO-SS-NHS) to the terminal primary amines of the tetra-arm PEGs. A detailed procedure for the synthesis can be found in the Supplementary Methods.

Cell culture. HEK293FT cells (Thermo Fisher) were cultured in chambered coverglasses (CultureWell, Thermo Fisher) to a confluency of 60–80% (ref. 1), before being fixed and immunostained^{14,8}. Briefly, the cells were treated with 3% (w/v) formaldehyde and 0.1% (w/v) glutaraldehyde in phosphate buffered saline (PBS; 1 \times unless otherwise noted) for 10 min at room temperature before the subsequent quenching, blocking, immunostaining and expansion procedures. HeLa cells (ATCC CCL-2) were plated on coverglasses coated with Matrigel (BD Sciences) to a confluency of 50–90% and fixed^{14,8,14}. The cells were treated with PBS with 3% (w/v) formaldehyde and 0.1% (w/v) glutaraldehyde for 10 min at room temperature before the subsequent quenching, blocking and expansion procedures. All of the cells were not subjected to additional authentication and were not tested for mycoplasma contamination. A detailed procedure for the immunostaining can be found in the Supplementary Methods.

Thy1-YFP mouse brain slice. All procedures involving Thy1-YFP-H transgenic mice (Jackson Laboratory) were performed in accordance with the US National Institutes of Health Guide for the Care and Use of Laboratory Animals and approved by the MIT Committee on Animal Care. All of the animals were housed in groups in standardized cages (temperature: 20–22°C, humidity: 30–70%) with a 12-hour light/12-hour dark cycle with unrestricted access to food and water. Coronal brain slices (50–100 μ m) of Thy1-YFP-H mice of 2–4 months old, both male and female, were prepared and immunostained for expansion^{4,8,13}. A detailed procedure for the immunostaining can be found in the Supplementary Methods.

General procedure for gelation, digestion and expansion. Fixed (and immunostained) cells and tissues were incubated in \sim 0.1–0.2 mg ml⁻¹ NHS-azide in PBS overnight at room temperature and washed with PBS twice. To form the gelling solution, the two monomer solutions were mixed at a close to 1:1 molar ratio and an additional amount of water was added to adjust the final concentration of monomer 1 to \sim 3.3% (w/v). For example, 10 μ l each of monomers 1 and 2' (both \sim 200 mg ml⁻¹) and 40 μ l of water were mixed to yield the gelling solution. Gelation was carried out for 1–2 h at 37°C (blank gels) or overnight at 4°C (cell and tissue samples) in a gelation chamber⁸. The gelled cell and tissue samples were incubated in digestion buffer with proteinase K (8 units ml⁻¹, 1:100 dilution; New England Biolabs) overnight at room temperature^{4,8} and expanded in an excess amount of water three times, each time for 20 min.

Expansion of HeLa cells (pre-expansion immunostaining and iterative expansion). Fixed HeLa cells were stained with primary antibodies, oligonucleotide-conjugated secondary antibodies and azide-modified tertiary oligonucleotides as previously described¹⁴. The cells were gelled with a cleavable TG gelling solution prepared by mixing monomers 1 and 2''' with water. The gelled samples were incubated in digestion buffer with proteinase K (8 units ml⁻¹) overnight at room temperature with gentle shaking before de-hybridization of the oligonucleotides from the gel-anchored oligonucleotides. The expanded samples were re-embedded in *N,N'*-bis(acryloyl)cystamine (BAC)-cross-linked non-expanding gel, hybridized with first linker oligonucleotides, re-embedded in *N,N'*-diallyl 1-tartardiamide (DATD)-cross-linked expanding gel, and incubated in BAC-cleaving buffer. For fluorescence readout, the samples were incubated with fluorophore-conjugated locked nucleic acid (LNA) oligonucleotides and expanded in water. A detailed procedure for the expansion can be found in the Supplementary Methods.

Expansion of HSV-1 virions (direct labelling and iterative expansion). Purified HSV-1 virion stock⁴⁷ was diluted before being drop-cast on to a plasma-cleaned #0 circular 12 mm coverslip. After 15 min of incubation at room temperature, the virions were fixed in 4% paraformaldehyde in PBS for 10 min. Azide-modified oligonucleotides were directly conjugated to the virion envelope proteins via SoluLink bioconjugation chemistry as previously described¹. The virions were gelled, digested, expanded and hybridized with fluorophore-conjugated LNA oligonucleotides using a similar procedure to that used for the HeLa cell expansion. For three-round iterative expansion, BAC-cleaved samples were re-embedded in DATD-cross-linked non-expanding gel, hybridized with second linker oligonucleotides, re-embedded in bis-cross-linked expanding gel and incubated in DATD-cleaving buffer before hybridization with the LNA oligonucleotide, expansion and imaging. A detailed procedure for the expansion and for the PAAG control can be found in the Supplementary Methods.

Expansion of HIV and VSV virions (direct labelling and iterative expansion). Purified HIV and VSV virions were immobilized, fixed, conjugated with oligonucleotides, gelled and then expanded following the two-round iterative expansion protocol of the HSV-1 virions.

Imaging and visualization. All the expanded samples were imaged with a diffraction-limited spinning disk confocal microscope (CSU-W1, Yokogawa on Eclipse Ti-E microscope body; Nikon) with a CFI Apo LambdaS LWD \times 40, 1.15 NA water-immersion objective (Nikon), controlled using NIS-Elements AR imaging software, v4.60.00 (Nikon). The two-colour HeLa cell images and all the virion images were deconvolved using theoretical point-spread-functions (Huygens Essential for MacX11 built on 7 Feb 2013; SVI) before visualization and image analysis. Unless otherwise noted, all the three-dimensional (3D) renderings were generated using Imaris \times 64 8.3 (Oxford Instruments). Part of the image datasets was analysed and visualized using ImageJ (Fiji) 2.10/1.53c. Part of the plots was generated using OriginPro8.1 (Origin).

Image analysis. For virion envelope protein analysis, first, single-particle averaged virion images were generated using a semi-automated image analysis pipeline⁴⁸ implemented on MATLAB R2018a–R2020b. Each virion was manually aligned, automatically cropped, calibrated with the expansion factor and arithmetically averaged to generate the single-particle averaged images. Next, spatial arrangements of the virion envelope proteins were quantified. Radii in eight directions (45° apart) were measured for each virion as the distance from the particle centroid to the Gaussian-fitted centre of the envelope profile. After inspection to remove unfitted profiles, standard deviations of all the accepted radii within the same particle (σ) were reported as population statistics for virions with \geq 3 accepted radii. For HSV-1 virion shape analysis, virions with \geq 6 accepted radii (for eccentricity measurements, virions with \geq 6 accepted radii and with the accepted radii constituting at least two mutually perpendicular diameters) were used to assure an accurate approximation of the particle shapes. The eccentricity (e) was defined as the ratio of the minor axis to the major axis. The sphericity (s) was defined as the ratio of the radius of the inscribing circle to the radius of the circumscribing circle. The normalized circular standard deviation (σ_c) was defined as the standard deviation of normalized radii (R_n) within each particle. For microtubule analysis, the peak-to-peak distance between the microtubule sidewalls was measured using a semi-automated algorithm⁴⁹ implemented on MATLAB R2018a–R2020b. On maximum intensity *z*-projection images of β -tubulin-stained HeLa cells, two points were manually selected along the centreline of a microtubule segment and a 200 nm (in biological length) segment was cropped out from the selected segment. The line intensity profile along the 200 nm segment was fitted with two Gaussian functions to detect the two peaks in the fluorescence intensity, between which the distance was measured as the peak-to-peak distance of the microtubule sidewalls. A detailed description of the image analysis can be found in the Supplementary Methods.

Modelling and simulation of single-particle averaged HSV-1 virion images. A model of spherical virions was developed on MATLAB R2020a–R2020b based on experimental parameters derived from individual HSV-1 virions, to simulate the single-particle averaged HSV-1 virion images⁵⁰ and their quantitative metrics. A detailed description of the modelling can be found in the Supplementary Methods.

Reporting Summary. Further information on research design is available in the Nature Research Reporting Summary linked to this article.

Data availability

Source data are provided with this paper. The total raw data size of the study exceeds 350 GB. The data that support this study are available from the authors upon reasonable request.

Code availability

Analysis code used in this study, including virus particle analysis⁴⁸, microtubule peak-to-peak distance analysis⁴⁹ and HSV-1 averaged particle image simulation⁵⁰ are available at <https://github.com/jayyu0528/>.

References

- Neve, R. L., Neve, K. A., Nestler, E. J. & Carlezon, W. A. Use of herpes virus amplicon vectors to study brain disorders. *Biotechniques* **39**, 381–391 (2005).
- Yu, C.-C. Virus particle analysis. *GitHub* <https://github.com/jayyu0528/> (2020).
- Yu, C.-C. Microtubule peak-to-peak distance analysis. *GitHub* <https://github.com/jayyu0528/> (2020).
- Yu, C.-C. HSV-1 averaged particle image simulation. *GitHub* <https://github.com/jayyu0528/> (2020).

Acknowledgements

We thank Y.-Y. Chou and T. Kirchhausen at HMS for help with VSV stock preparation and virion immobilization; C. Linghu and O. Shemesh for help with HSV-1 stock preparation; P. Valdes and C. Zhang for helpful discussion about sample staining

and expansion; M. J. Kauke for helpful discussion about DNA staining; S. M. Asano for helpful discussion about image analysis; G. H. Huynh for help with mouse brain slice preparation; F. Chen for helpful discussion about monomer and polymerization chemistry design; R. Herlo at HMS for helpful discussion about virion envelope proteins. E.S.B. acknowledges L. Yang and Y. E. Tan, J. Doerr, the Open Philanthropy Project, NIH 1R01NS087950, NIH 1RM1HG008525, NIH 1R01DA045549, NIH 2R01DA029639, NIH 1R01NS102727, NIH 1R01EB024261, NIH 1R01MH110932, the HHMI-Simons Faculty Scholars Program, the HHMI Investigator program, IARPA D16PC00008, the US Army Research Laboratory and the US Army Research Office under contract/grant W911NF1510548, the US-Israel Binational Science Foundation Grant 2014509, NSF Grant 1734870 and the NIH Director's Pioneer Award 1DP1NS087724. C.-C.Y. acknowledges the McGovern Institute for Brain Research at MIT for the Friends of the McGovern Fellowship. S.U. was supported by Biogen and NIH 5R01GM075252-13S grants awarded to T. Kirchhausen, and acknowledges support from Philomathia Foundation and Chan Zuckerberg Initiative Imaging Scientist program.

Author contributions

R.G. and L.G. designed and synthesized the monomers and conducted initial gelation experiments. C.-C.Y. and R.G. designed and conducted iterative expansion, virion expansion and associated analysis. C.-C.Y. created the semi-automated virion analysis pipeline and the simulation model. K.D.P. helped characterization of the gel in cell

culture. R.L.N. purified HSV-1 and prepared the virion stock solution. J.B.M. provided purified HIV virions. S.U. provided purified VSV virions and conducted initial virion immobilization experiments. C.-C.Y., R.G. and L.G. processed and performed quantitative analysis of all image data. R.G., C.-C.Y. and E.S.B. wrote the manuscript with input from all co-authors. E.S.B. supervised the project.

Competing interests

R.G., C.-C.Y., L.G. and E.S.B. have filed for patent protection on a subset of the technologies here described. E.S.B. is a cofounder of a company that aims to commercialize ExM for medical purposes. R.G., C.-C.Y., L.G. and E.S.B. are co-inventors on multiple patents related to ExM. The authors declare no other competing interests.

Additional information

Supplementary information The online version contains supplementary material available at <https://doi.org/10.1038/s41565-021-00875-7>.

Correspondence and requests for materials should be addressed to E.S.B.

Peer review information *Nature Nanotechnology* thanks the anonymous reviewers for their contribution to the peer review of this work.

Reprints and permissions information is available at www.nature.com/reprints.

Reporting Summary

Nature Research wishes to improve the reproducibility of the work that we publish. This form provides structure for consistency and transparency in reporting. For further information on Nature Research policies, see our [Editorial Policies](#) and the [Editorial Policy Checklist](#).

Statistics

For all statistical analyses, confirm that the following items are present in the figure legend, table legend, main text, or Methods section.

n/a Confirmed

- The exact sample size (n) for each experimental group/condition, given as a discrete number and unit of measurement
- A statement on whether measurements were taken from distinct samples or whether the same sample was measured repeatedly
- The statistical test(s) used AND whether they are one- or two-sided
Only common tests should be described solely by name; describe more complex techniques in the Methods section.
- A description of all covariates tested
- A description of any assumptions or corrections, such as tests of normality and adjustment for multiple comparisons
- A full description of the statistical parameters including central tendency (e.g. means) or other basic estimates (e.g. regression coefficient) AND variation (e.g. standard deviation) or associated estimates of uncertainty (e.g. confidence intervals)
- For null hypothesis testing, the test statistic (e.g. F , t , r) with confidence intervals, effect sizes, degrees of freedom and P value noted
Give P values as exact values whenever suitable.
- For Bayesian analysis, information on the choice of priors and Markov chain Monte Carlo settings
- For hierarchical and complex designs, identification of the appropriate level for tests and full reporting of outcomes
- Estimates of effect sizes (e.g. Cohen's d , Pearson's r), indicating how they were calculated

Our web collection on [statistics for biologists](#) contains articles on many of the points above.

Software and code

Policy information about [availability of computer code](#)

Data collection Fluorescence microscopy data were recorded using NIS-Elements AR v4.60.00 (Nikon).

Data analysis Virion data were analyzed using "Virus Particle Analysis", a custom code implemented on MATLAB R2018a, R2018b, R2019a, R2019b, R2020a, and R2020b. Simulation of HSV-1 virion images was performed using "HSV-1 Averaged Particle Image Simulation", a custom code implemented on MATLAB R2020a and R2020b. Microtubule data were analyzed using "Microtubule Peak-to-Peak Distance Analysis", a custom code implemented on MATLAB R2018a, R2018b, R2019a, R2019b, R2020a, and R2020b. Part of the image datasets were deconvolved using Huygens Essential for MacX11 built on Feb 7, 2013 (SVI). Part of the image datasets were analysed, visualized, and/or 3D rendered using Imaris x64 8.3 (Oxford Instruments) and ImageJ (Fiji) 2.10/1.53c. Part of the plots were generated using OriginPro8.1 (Origin).

Code availability: The "Virus Particle Analysis", "HSV-1 Averaged Particle Image Simulation", and "Microtubule Peak-to-Peak Distance Analysis" are available at "https://github.com/jayyu0528/".

For manuscripts utilizing custom algorithms or software that are central to the research but not yet described in published literature, software must be made available to editors and reviewers. We strongly encourage code deposition in a community repository (e.g. GitHub). See the Nature Research [guidelines for submitting code & software](#) for further information.

Data

Policy information about [availability of data](#)

All manuscripts must include a [data availability statement](#). This statement should provide the following information, where applicable:

- Accession codes, unique identifiers, or web links for publicly available datasets
- A list of figures that have associated raw data
- A description of any restrictions on data availability

Data availability: The data that support this study are available from the authors upon reasonable request.

Field-specific reporting

Please select the one below that is the best fit for your research. If you are not sure, read the appropriate sections before making your selection.

- Life sciences Behavioural & social sciences Ecological, evolutionary & environmental sciences

For a reference copy of the document with all sections, see [nature.com/documents/nr-reporting-summary-flat.pdf](https://www.nature.com/documents/nr-reporting-summary-flat.pdf)

Life sciences study design

All studies must disclose on these points even when the disclosure is negative.

| | |
|-----------------|---|
| Sample size | The sample size used in the study was based on our past experience as well as previous studies in the field that developed similar imaging technologies (e.g., Nat. Methods 16, 71–74 (2019), Nat. Methods 14, 593–599 (2017), Nat. Biotechnol. 34, 987–992 (2016), and Nat. Methods 13, 485–488 (2016)). |
| Data exclusions | For single-particle averaged virion images and spatial analyses of virion envelope proteins, virions with significant overlaps with neighboring virions (<10% of all virions) were excluded from the averaging and analysis. For the virion radius analysis, radii (1) containing peaks that belonged to other virions, (2) in the direction that was not present or was significantly dimmer than that in other directions, or (3) to which the automated Gaussian fitting failed, were excluded. For the HSV-1 virion shape analysis, virions that do not meet the criteria to accurately define a particular shape descriptor were excluded. All the exclusion criteria were pre-established. Detailed descriptions of the criteria are provided in the Supplementary Methods. |
| Replication | Unless otherwise noted, all data shown were obtained from at least 3 biological independent replicates. For virion analysis, all the HSV-1 and HIV virions used for the two types of gels were from a single batch of live HSV-1 and HIV preparation, respectively. For representative images, unless otherwise noted, each experiment was successfully repeated at least three times under similar conditions, and the results shown are representative of the repeats. |
| Randomization | This is not relevant as no treatment assignments or experimental group allocations were involved in the study. All the biological samples were allocated to a single experimental group and examined as they got embedded in and expanded by hydrogels. |
| Blinding | This is not relevant as no treatment assignments or experimental group allocations were involved in the study. All the biological samples were allocated to a single experimental group and examined as they got embedded in and expanded by hydrogels. |

Reporting for specific materials, systems and methods

We require information from authors about some types of materials, experimental systems and methods used in many studies. Here, indicate whether each material, system or method listed is relevant to your study. If you are not sure if a list item applies to your research, read the appropriate section before selecting a response.

Materials & experimental systems

| n/a | Involvement in the study |
|-------------------------------------|---|
| <input type="checkbox"/> | <input checked="" type="checkbox"/> Antibodies |
| <input type="checkbox"/> | <input checked="" type="checkbox"/> Eukaryotic cell lines |
| <input checked="" type="checkbox"/> | <input type="checkbox"/> Palaeontology and archaeology |
| <input type="checkbox"/> | <input checked="" type="checkbox"/> Animals and other organisms |
| <input checked="" type="checkbox"/> | <input type="checkbox"/> Human research participants |
| <input checked="" type="checkbox"/> | <input type="checkbox"/> Clinical data |
| <input checked="" type="checkbox"/> | <input type="checkbox"/> Dual use research of concern |

Methods

| n/a | Involvement in the study |
|-------------------------------------|---|
| <input checked="" type="checkbox"/> | <input type="checkbox"/> ChIP-seq |
| <input checked="" type="checkbox"/> | <input type="checkbox"/> Flow cytometry |
| <input checked="" type="checkbox"/> | <input type="checkbox"/> MRI-based neuroimaging |

Antibodies

Antibodies used

Primary antibodies: rat anti-alpha-tubulin antibody (MA1-80017, Thermo Fisher, 1:200); rabbit anti-Homer1 antibody (160003, Synaptic Systems, 1:200); chicken anti-GFP antibody (A10262, Thermo Fisher, 1:200); rabbit anti-beta-tubulin (ab6046, Abcam,

1:100); sheep anti-alpha/beta tubulin (ATN02, Cytoskeleton, 1:50); rabbit anti-clathrin heavy chain (ab21679, Abcam, 1:500).

Secondary antibodies: Alexa Fluor 488-conjugated donkey anti-rat antibody (A-21208, Thermo Fisher, 1:200); Alexa Fluor 647-conjugated goat anti-rabbit antibody (A21245, Thermo Fisher, 1:200); Cy5-conjugated goat anti-rabbit antibody (A10523, Thermo Fisher, 1:200); Alexa Fluor 680-conjugated goat anti-rabbit antibody (A21109, Thermo Fisher, 1:200); Alexa Fluor 488-conjugated goat anti-chicken antibody (A11039, Thermo Fisher, 1:200); donkey anti-rabbit antibody (711-005-152, Jackson ImmunoResearch, 10 microgram/mL final concentration); donkey anti-sheep antibody (713-005-147, Jackson ImmunoResearch, 10 microgram/mL final concentration).

Validation

Detailed analysis and species validation of the primary antibodies can be found on, for example, the following vendor websites.

Rat anti-alpha-tubulin antibody (MA1-80017, Thermo Fisher): https://assets.thermofisher.com/TFS-Assets/LSG/certificate/Certificates-of-Analysis/MA180017_147397.PDF

Rabbit anti-Homer1 antibody (160003, Synaptic Systems): https://sysy.com/product-factsheet/SySy_160003

Chicken anti-GFP antibody (A10262, Thermo Fisher): <https://www.thermofisher.com/antibody/product/GFP-Antibody-Polyclonal/A10262>

Rabbit anti-beta-tubulin (ab6046, Abcam): <https://www.abcam.com/beta-tubulin-antibody-loading-control-ab6046.pdf>

Sheep anti-alpha/beta tubulin (ATN02, Cytoskeleton): <https://www.cytoskeleton.com/pdf-storage/datasheets/atn02.pdf>

Rabbit anti-clathrin heavy chain (ab21679, Abcam): <https://www.abcam.com/clathrin-heavy-chain-antibody-ab21679.pdf>

Eukaryotic cell lines

Policy information about [cell lines](#)

Cell line source(s)

HEK293FT (Thermo Fisher) and HeLa (ATCC CCL-2) cells.

Authentication

Cells were not subjected to additional authentication.

Mycoplasma contamination

Cells were not tested for mycoplasma contamination.

Commonly misidentified lines
(See [ICLAC](#) register)

None.

Animals and other organisms

Policy information about [studies involving animals](#); [ARRIVE guidelines](#) recommended for reporting animal research

Laboratory animals

Mice (Thy1-YFP-H strain, Jackson Laboratory), 2-4 months old, both male and female.

Wild animals

None.

Field-collected samples

None.

Ethics oversight

The Massachusetts Institute of Technology Committee on Animal Care.

Note that full information on the approval of the study protocol must also be provided in the manuscript.

Supplementary information

A highly homogeneous polymer composed of tetrahedron-like monomers for high-isotropy expansion microscopy

In the format provided by the authors and unedited

A highly homogeneous polymer composed of tetrahedron-like monomers for high-isotropy expansion microscopy

Ruixuan Gao, Chih-Chieh (Jay) Yu, Linyi Gao, Kiryl D Piatkevich, Rachael L Neve, James B Munro, Srigokul Upadhyayula & Edward S Boyden

Supplementary Information

Supplementary Methods
Supplementary Figs. 1-8
Supplementary Tables 1-3

Supplementary Methods

Synthesis of tetra-arm sodium polyacrylate with azide terminal groups (**1**) (monomer **1**)

Monomer **1** was synthesized using a modified procedure as previously described³⁰ (**Supplementary Fig. 1**). Unless otherwise noted, all chemicals were procured from Sigma Aldrich.

First, tetra-arm poly(*t*-butyl acrylate) with bromo terminal groups (**4**) was synthesized by atom transfer radical polymerization (ATRP). Before the synthesis, *t*-butyl acrylate was purified with an inhibitor removal column to remove a trace amount of 4-methoxyphenol. Next, 128 mL of the purified *t*-butyl acrylate was added to 640 mg of copper (I) bromide and 48 mg of copper (II) bromide, and the mixture was bubbled with dry nitrogen at 50 °C before 1.03 mL of *N,N,N',N'',N'''*-pentamethyl diethylenetriamine (PMDETA) was added dropwise. After 5-10 min of continuous bubbling and stirring, a 16 mL acetone solution of 1.6 g pentaerythritol tetrakis(2-bromoisobutyrate) (**3**) was added dropwise. The reaction mixture was stirred at 50 °C for 90 min, with dry nitrogen bubbling on for the first ~10 min. After the reaction, unreacted *t*-butyl acrylate was removed by rotary evaporation before the crude product mixture was dissolved in dimethylformamide (DMF) and precipitated with water. The precipitation was repeated two to three times additionally, yielding 15.3 g of tetra-arm poly(*t*-butyl acrylate) with bromo terminal groups (**4**) as a white powder.

Next, tetra-arm poly(*t*-butyl acrylate) with azide terminal groups (**5**) was synthesized by replacing bromines of **4** with azides. 15.3 g of **4** was dissolved in 80 mL of DMF and an excess amount of sodium azide (exceeding its solubility in DMF) was added to the reaction mixture. The reaction was carried out overnight at room temperature and the supernatant was subsequently decanted and precipitated with water, yielding 11.0 g of tetra-arm poly(*t*-butyl acrylate) with azide terminal groups (**5**) as a white powder. Using the ratio between the core/end and backbone H in the ¹H NMR spectra of **5**, the average number of *t*-butyl acrylate units and the average molecular weight of **5** was determined to be $n = 21.22$ and ~11522, respectively (**Supplementary Fig. 2**). In addition, the end to core H ratio (>50%) in the same spectra suggested a close to 100% conversion rate for the azide terminal groups.

Finally, monomer **1** was synthesized by hydrolysis and neutralization of **5**. A total of 5.04 g of **5** was dissolved in 30 mL of methylene chloride, followed by addition of 15 mL of trifluoroacetic acid (TFA). The hydrolysis was carried out at 4 °C with gradual precipitation of a white powder. After 24-48 hours, the precipitated product was collected by centrifugation, washed with acetone, and dried in a low-humidity chamber. The product was re-suspended in an aqueous solution of sodium hydroxide to yield monomer **1** solution (~200 mg/mL) at a final pH of ~7.

Synthesis of tetra-arm polyethylene glycol (PEG) with dibenzocyclooctyne (DBCO, **2'**), bicyclo[6.1.0]non-2-yne (BCN, **2''**), and dibenzocyclooctyne-disulfide (DBCO-SS, **2'''**) terminal groups (monomer **2**)

DBCO-, BCN- and DBCO-SS-terminated monomers **2'**, **2''**, and **2'''** were synthesized by *N*-hydroxysuccinimide (NHS) ester-based conjugation of the alkynes to the terminal primary amines of tetra-arm PEGs. First, amine-terminated tetra-arm PEG (~10 kDa for **2'** and **2''**; ~20

kDa for 2'''; NOF Corp.) was dissolved in dimethyl sulfoxide (DMSO) to a concentration of 100-200 mg/mL. The average molecular weight and the terminal activity was ~11069 and ~93.4% for the ~10 kDa tetra-arm PEG, and ~20086 and ~95.9% for the ~20 kDa tetra-arm PEG, respectively. Next, DBCO-NHS, BCN-NHS or DBCO-SS-NHS was added to the DMSO solution at a 1:1 molar ratio to the total number of terminal amines of the tetra-arm PEGs. Finally, the conjugation reaction was carried out overnight at room temperature to the yield monomer 2', 2'', or 2''' solutions.

HEK293 cells

HEK293FT cells (Thermo Fisher) were cultured in chambered coverglasses (CultureWell, Thermo Fisher) to a confluency of 60-80% as previously described¹. The cells were then fixed and immunostained^{1,4,8}. Briefly, the cells were treated with 3% (w/v) formaldehyde and 0.1% (w/v) glutaraldehyde in phosphate buffered saline (PBS; here and after, 1x unless otherwise noted) for 10 min, quenched with 0.1% NaBH₄ (w/v) in PBS for 7 min, and then with 100 mM glycine in PBS for 10 min. Immediately after fixation, the cells were permeabilized with 0.1% (w/w) Triton X-100 in PBS for 15 min and blocked with a blocking buffer [5% (v/v) normal donkey serum (NDS) and 0.1% (w/w) Triton X-100 in PBS] for 15 min. For primary antibody staining, the cells were incubated in rat anti-alpha-tubulin antibody (MA1-80017, Thermo Fisher) solution (1:200 dilution with the blocking buffer) overnight and were washed with the blocking buffer three times, each time for 5 min. For secondary antibody staining, the cells were incubated in Alexa Fluor 488-conjugated donkey anti-rat antibody (A-21208, Thermo Fisher) solution (1:200 dilution with the blocking buffer) for 5 hours and were washed with the blocking buffer three times, each time for 5 min. Finally, the cells were washed with PBS once for 5 min and stored in PBS for the subsequent expansion procedure. Unless otherwise noted, all the incubation and washing steps were carried out at room temperature. All the cells were not subjected to additional authentication and were not tested for mycoplasma contamination.

HeLa cells

HeLa cells (ATCC CCL-2) were plated on coverglasses coated with Matrigel (BD Sciences) to a confluency of 50-90% and then fixed^{1,4,8,14}. Briefly, cells were treated with PBS + 3% (w/v) formaldehyde + 0.1% (w/v) glutaraldehyde for 10 min, quenched with PBS + 0.1% (w/v) NaBH₄ for 7 min. The cells were then washed once with PBS + 100 mM glycine for 5 min, and then twice with PBS for 5 min each. Fixed cells were stored at 4°C until the immunostaining step. Unless otherwise noted, all the incubation and washing steps were carried out at room temperature. All the cells were not subjected to additional authentication and were not tested for mycoplasma contamination.

Thy1-YFP mouse brain slices

All procedures involving transgenic mice expressing cytosolic YFP under Thy1 promoter (Thy1-YFP-H strain, Jackson Laboratory) were carried out in accordance with the US National Institutes of Health Guide for the Care and Use of Laboratory Animals and approved by the MIT Committee on Animal Care. All the animals were housed in group in standardized cages (temperature: 20-22 °C, humidity: 30-70%) with a 12-hour light/12-hour dark cycle with unrestricted access to food and water. Coronal brain slices of the Thy1-YFP-H mice were prepared and immunostained^{4,8,13}. Unless otherwise noted, all the incubation and washing steps

were carried out at room temperature. Briefly, Thy1-YFP-H mice, 2-4 months old, both male and female, were anesthetized with ketamine/xylazine and perfused transcardially with 25 mL ice cold 4% (w/v) paraformaldehyde (PFA) in PBS, followed by 25 mL of ice-cold PBS. The brains were dissected out and soaked in 4% (w/v) PFA in PBS for 24 hours at 4°C. 50-100 µm coronal slices were prepared using a vibratome (Leica VT1000S) and were stored in PBS at 4 °C for the subsequent expansion procedure.

For pre-expansion staining, the fixed brain slices were permeabilized and blocked with a blocking buffer [5% (v/v) NDS and 0.1% (w/w) Triton X-100 in PBS] for 2 hours. For primary antibody staining, the slices were incubated with rabbit anti-Homer1 antibody (160003, Synaptic Systems) solution (1:200 dilution with the blocking buffer) overnight and washed with the blocking buffer twice, each time for 30 min. For secondary antibody staining, the slices were incubated with dye-conjugated Alexa Fluor 647, Cy5, or Alexa Fluor 680 goat anti-rabbit antibody (A21245, A10523, or A21109, Thermo Fisher) solution (1:200 dilution with the blocking buffer) overnight and washed with the blocking buffer twice, each time for 30 min. Finally, the slices were washed once with PBS and stored in PBS for the subsequent expansion procedure.

For post-proteolysis staining, the gelled and digested brain slices were incubated with chicken anti-GFP antibody (A10262, Thermo Fisher) solution (1:200 dilution with the blocking buffer) overnight and subsequently with Alexa Fluor 488-conjugated goat anti-chicken antibody (A11039, Thermo Fisher) solution (1:200 dilution with the blocking buffer) overnight before the same washing and storage steps with PBS as described.

Gelation, digestion, and expansion of cells and tissues (single-round expansion)

Unless otherwise noted, single-round expansion of cells and tissues with tetra-gel (TG) was carried out using the following general procedure.

First, fixed (and immunostained) cells and tissues were incubated in ~0.1-0.2 mg/mL NHS-azide in PBS overnight at room temperature and washed with PBS twice immediately before gelation.

Next, monomer **1** and monomer **2** solutions were mixed at close to 1:1 molar ratio, and an additional amount of water was added to adjust the final concentration of monomer **1** to ~3.3% (w/v) (**Supplementary Table 2**). In a typical gelation with monomer **2'**, 10 µL of monomer **1** (~200 mg/mL), 10 µL of monomer **2** (~200 mg/mL), and 40 µL of water were mixed to yield the gelling solution. We note that the molar ratio between the mixed monomer **1** and **2'** can vary slightly according to the molecular weight of monomer **1**, which depends on the final conversion rate of the t-butyl ester hydrolysis in the last deprotection step of the synthesis. For example, the exact molar ratio of monomer **1** to **2'** can be ~0.99 at 50% conversion and ~1.16 at 100% conversion. After drop-casting the gelling solution to the samples in a gelation chamber as previously described^{4,8}, gelation was carried out for 1-2 hours at 37 °C (blank gels) or overnight at 4 °C (cell and tissue samples). The total amount of monomers being mixed was adjusted proportionally according to the size and number of the samples. The time-resolved gelation assay was carried out by gently touching the gelling solution (~30-60 µL, 4 °C) in a small PCR tube with a thin pipette tip at different time points from the monomer mixing. For reference,

additional gelling conditions that were tested but were not used for cell or tissue samples are provided in **Supplementary Table 3**.

Finally, the gelled cell and tissue samples were incubated in the digestion buffer with Proteinase K (8 units/mL) (New England BioLabs; 1:100 dilution) overnight at room temperature as previously described^{4,8}. For expansion, the digested samples were washed in an excess amount of water three times, each time for 20 min.

For fluorescein visualization of blank gels, a trace amount of fluorescein amine was mixed into the gelling solution. Briefly, a stock solution of ~50 mM fluorescein-azide was prepared by adding 5 μ L of 100 mM fluorescein-amine in DMSO to 5 μ L of 20 mg/mL NHS-azide in DMSO. ~3 μ L of the fluorescein-azide stock solution was added to ~60 μ L of the gelling solution (with monomer **2'**, **2''**, or **2'''**). The gelling solution with fluorescein was drop-casted into a circular mold of ~3 mm diameter before gelation for 1-2 hours at 37 °C.

Expansion of HeLa cells (pre-expansion immunostaining and iterative expansion)

Pre-expansion immunostaining

Fixed cells were stained with primary antibodies, oligo-conjugated secondary antibodies, and azide-modified tertiary oligos as previously described^{1,14}. Briefly, fixed cells were permeabilized and blocked with HeLa staining buffer [PBS + 5% (v/v) NDS + 0.2% (w/w) Triton X-100] for 10 min. Primary antibody staining was performed with HeLa staining buffer for 1 hour at room temperature, followed by 3 washes with PBS for 5 min each at room temperature. Secondary antibody staining was performed with hybridization buffer [10% w/v dextran sulfate, 1 mg/mL yeast tRNA, 5% (v/v) NDS, 2x SSC, 0.1% (w/w) Triton X-100] for 1 hour at room temperature, followed by 3 washes with PBS for 5 min each at room temperature. Tertiary oligo hybridization was performed by first incubating the sample in hybridization buffer for 3 hours, followed by incubation with the tertiary oligo overnight at room temperature. After hybridization, samples were washed with PBS three times for 5 min each at room temperature. For single-color tubulin staining, the cells were stained with rabbit anti-beta-tubulin (ab6046, Abcam, 1:100 dilution) primary antibody, and then with oligo-conjugated donkey anti-rabbit secondary antibody (711-005-152, Jackson ImmunoResearch, 10 μ g/mL final concentration; oligo sequence B1'; see **Supplementary Table 1** for oligo sequences used), followed by hybridization with azide-modified complementary oligo (oligo sequence B1, at 100 nM). For dual-colour tubulin and clathrin staining, the cells were stained with sheep anti-alpha/beta tubulin (ATN02, Cytoskeleton, Inc, 1:50 dilution) and rabbit anti-clathrin heavy chain (ab21679, Abcam, 1:500 dilution) primary antibodies, and then with oligo-conjugated donkey anti-sheep (711-005-147, Jackson ImmunoResearch, 10 μ g/mL final concentration; oligo sequence A2') and donkey anti-rabbit (711-005-152, Jackson ImmunoResearch, 10 μ g/mL final concentration; oligo sequence B1') secondary antibodies, followed by hybridization with azide-modified complementary oligos (oligo sequences B1 and A2, at 100 nM each). Oligo-conjugation to the secondary antibodies were performed with the same protocol as previously described¹ (also available on www.expansionmicroscopy.org), with the modification that the S-HyNic reaction was performed with three times of its concentration (600 μ M instead of 200 μ M) compared to the original protocol.

Gelation and digestion

As described in the previous section, the cleavable TG gelling solution was prepared by mixing monomer **1** (200 mg/mL) and monomer **2''''** (200 mg/mL) at a molar ratio of close to 1:1 and then adding water to adjust the final concentration of monomer **1** to ~3.3% (w/v) (**Supplementary Table 2**). A gelation chamber was constructed around the cell-immobilized coverslip using the following steps. First, the coverslip was transferred to the centre of a glass slide. Spacers consisting of a stack of one #0 and one #1 coverslip were placed on either side of the cell-immobilized coverslip. 50 μ L of freshly prepared TG gelling solution was added to the coverslip, and the chamber was closed by placing a rectangular coverslip on top of the spacers. The gelling solution was further added from the side of the chamber until the chamber was completely filled. Gelation chambers were then placed in a humidified chamber and incubated at 4 °C overnight. After the incubation, the chamber was partially opened using a diamond scribe to remove portions of the top coverslip that were not directly above the cell-immobilized coverslip. The chamber was then placed into a rectangular 4-well dish and incubated in digestion buffer with Proteinase K at 8 units/mL (1:100 dilution) overnight at room temperature with gentle shaking. The diameter of the gel was measured for downstream estimation of the overall expansion factor. Regions inside the circular 12-mm coverslip (i.e., regions with the immobilized cells) were trimmed into a parallelogram, of which the side lengths were measured for downstream estimation of the overall expansion factor. Finally, trimmed gels were washed twice in PBS, each time for 10 min. To de-hybridize B1' and A2' oligos (conjugated to the secondary antibodies) from the gel-anchored B1 and A2 oligos (the azide-modified tertiary oligos), the gels were incubated in 80% (v/v) formamide at room temperature for 1 hour with gentle shaking, and then washed three times in PBST [PBS + 0.1% (w/w) Triton X-100] at room temperature with gentle shaking, for 30 min each.

Re-embedding into a BAC-crosslinked non-expanding 2nd gel

The gels were transferred (with the cell side facing down) into a rectangular 4-well dish that carries a glass slide in each well, and expanded in water three times, each time for 30 min. The gels were then incubated in 3 mL of BAC-crosslinked non-expanding gelling solution [10.4% (w/v) acrylamide, 0.2% (w/v) BAC, 0.05% (w/v) TEMED, 0.05% (w/v) APS] for 5 min with gentle shaking. After the incubation, the non-expanding gelling solution was removed from the well, and the glass slide carrying the expanded gel was transferred to a gelation chamber. Spacers consisting of a stack of two #1.5 coverslips were placed on either side of the gel, and the chamber was closed with a rectangular coverslip. The non-expanding gelling solution was added from the side of the chamber until the chamber was completely filled. The gelation chambers were incubated for 2 hours at 37 °C. After gelation, the chambers were opened by removing the top coverslip. Side lengths of the parallelogram were measured. The gels were trimmed to leave only the portion inside the parallelogram, while preserving the shape of the parallelogram. Side lengths of the trimmed gels were measured. Finally, the trimmed gels were washed twice in PBS, each time for 30 min.

1st Linker hybridization

The gels were incubated in hybridization buffer [4x SSC + 20% (v/v) formamide] for 30 min at room temperature. The gels were incubated with 1 nmol of oligo 5'Ac-B1'-4xB2' in 1 mL of hybridization buffer overnight at room temperature. After incubation, the gels were washed in hybridization buffer three times, each time for 1 hour, and then overnight, all with gentle shaking. The gels were then washed three times in PBS, each time for 5 min.

Re-embedding into a DATD-crosslinked expanding 3rd gel

The gels were incubated in DATD-crosslinked expanding gelling solution [8.6% (w/v) sodium acrylate, 2.6% (w/v) acrylamide, 0.5% (w/v) DATD, PBS, 2M NaCl, 0.01% (w/v) 4-HT, 0.2% (w/v) TEMED, 0.2% (w/v) APS] for 30 min at 4 °C. The gels (with the cell side facing down) were then enclosed in gelation chambers, incubated for 2 hours at 37 °C, size-measured, trimmed, size-re-measured, and washed as described in “*Re-embedding into a BAC-crosslinked non-expanding 2nd gel*”.

Cleaving BAC-crosslinked 1st and 2nd gels

The gels were incubated in BAC-cleaving buffer (0.25M TCEP-HCl, 0.75M Tris-HCl, pH 8.0) overnight at room temperature. The gels were then washed four times in PBS, each time for 30 min.

LNA hybridization for readout after 2-round expansion

The gels were incubated with 1 nmol of fluorophore-conjugated LNA oligo (LNA_B2-Atto647N and/or LNA_A1-Atto565; see sequences in **Supplementary Table 1**) in 500 µL of hybridization buffer. The LNA-hybridized gels were washed in hybridization buffer three times, each time for 1 hour, and then overnight, all with gentle shaking. The gels were then washed three times in PBS, each time for 5 min.

Gel expansion, immobilization, and imaging for 2-round expanded samples

The gels were trimmed into smaller pieces (~5 by 5 mm) while preserving the shape of the parallelogram. First, the gels were transferred (with the cell side facing down) into a rectangular 4-well dish that carries a glass slide in each well, and expanded in water three times, each time for 30 min. A glass-bottom 6-well plate was modified with poly-lysine, and the expanded gels were gently transferred to the poly-lysine modified coverslip surface for imaging, as previously described⁴.

Expansion of HSV-1 virions (direct labelling and iterative expansion)

Immobilization and fixation

Purified HSV-1 virion stock was prepared by the Viral Core Facility at the Massachusetts General Hospital (MGH) as previously described⁴⁷. The HSV-1 stock was diluted to a titer of 2.5×10^8 functional virions/mL in PBS and kept on ice until immobilization. A #0 circular 12-mm coverslip was cleaned with a plasma cleaner (PDC-001, Harrick Plasma) for 1 min. Immediately after the plasma cleaning, 30 µL of the diluted HSV-1 solution was drop-casted onto the coverslip and incubated for 15 min at room temperature. The immobilized virions were fixed in 4% PFA in PBS for 10 min, and then washed with PBS twice, each time for 5 min.

Oligo-conjugation to envelope proteins

Envelope proteins on the fixed virions were conjugated to DNA oligos with the SoluLink bioconjugation chemistry as previously described¹. The oligo provided a molecular handle for label anchoring, transfer, and amplification through the iterative expansion process. Briefly, a 22-bp oligo [sequence B1' with a 5' amine modification¹⁴ (Integrated DNA Technologies)] was purified with ethanol precipitation and reacted with Sulfo-S-4FB (S4FB) overnight in Buffer A (150 mM NaCl, 100 mM Na₂HPO₄, pH 7.4) at a molar ratio of 1:15. The S4FB-reacted oligo

was purified with a size exclusion filter, and then stored at 4 °C. Fixed virions immobilized on the coverslip were washed in Buffer A for 5 min, and then incubated with 100 µL of 160 mM S-HyNic in Buffer A for 2 hours at room temperature. The S-HyNic-reacted virions were washed with Buffer C (150 mM NaCl, 100 mM Na₂HPO₄, pH 6.0) twice, each time for 5 min. Oligo-conjugation solution was prepared by first adding 50 nmol of purified S4FB-reacted oligo to 100 µL of Buffer C, and then adding an amount of 10x TurboLink Catalyst Buffer that equals to 1/9 of the combined volume. The S-HyNic-reacted virions were incubated in the oligo-conjugation buffer overnight at room temperature in a humidified chamber. Next, the oligo-conjugated virions were washed three times with PBS, each time for 10 min, and then incubated in detergent-free hybridization buffer [10% (w/v) dextran sulfate, 1 mg/mL yeast tRNA, 5% (v/v) NDS, 2x SSC] for 3 hours at room temperature. The virions were incubated with 4 nmol of oligo B1-azide (or oligo B1-acrydite) for the subsequent gelation with TG [or sodium polyacrylate/polyacrylamide gel (PAAG) as control], in 300 µL of the detergent-free hybridization buffer, overnight at room temperature. For B1-acrydite, 5'acrydite-B1 was used. For B1-azide, TG with 3'Azide-B1 was found to yield slightly larger spatial errors compared to TG with 5' Azide-B1 (using the virion envelope protein spatial analysis described later). Despite the difference in the anchor placement with the B1-acrydite, 3' Azide-B1 was used for the final HSV-1 virion expansion and subsequent analysis of spatial errors to keep our isotropy analysis more conservative against TG (as 3'Azide-B1 yields comparatively larger spatial errors, i.e., lower isotropy). Finally, the virions were washed three times in PBS, each time for 10 min.

Gelation and digestion

As described in the previous section, cleavable TG gelling solution was prepared by mixing monomer **1** (200 mg/mL) and monomer **2'''** (200 mg/mL) at a molar ratio of close to 1:1 and then adding water to adjust the final concentration of monomer **1** to ~3.3% (w/v) (**Supplementary Table 2**). BAC-crosslinked cleavable sodium polyacrylate/polyacrylamide gel gelling solution was prepared for PAAG control as previously described¹⁴. A gelation chamber was constructed around the virion-immobilized coverslip using the following steps. First, the coverslip was transferred to the centre of a glass slide. Spacers consisting of a stack of one #0 and one #1 coverslip were placed on either side of the virion-immobilized coverslip. 50 µL of freshly prepared TG (or PAAG) gelling solution was added to the coverslip, and the chamber was closed by placing a rectangular coverslip on top of the spacers. The gelling solution was further added from the side of the chamber until the chamber was completely filled. After gelation for 2 hours at 37 °C, the chamber was partially opened using a diamond scribe to remove portions of the top coverslip that were not directly above the virion-immobilized coverslip. The chamber was then placed into a rectangular 4-well dish and incubated in digestion buffer with Proteinase K at 8 units/mL (1:100 dilution) overnight at room temperature with gentle shaking. After digestion, the top coverslip came off naturally and was removed from the solution. The diameter of the gel was measured for downstream estimation of the overall expansion factor. Regions inside of the circular 12-mm coverslip (i.e., regions with the immobilized virions) were trimmed into a parallelogram, of which the side lengths were measured for downstream estimation of the overall expansion factor. Finally, trimmed gels were washed twice in PBS, each time for 10 min. To de-hybridize B1' and B1 oligos, the gels were incubated in 80% (v/v) formamide at room temperature with gentle shaking for 1 hour, and then washed three times in PBS, each time for 10 min.

Re-embedding into a BAC-crosslinked non-expanding 2nd gel

The gels were transferred (with the virion side facing down) into a rectangular 4-well dish that carries a glass slide in each well, and expanded in water three times, each time for 30 min. The gels were then incubated in 3 mL of BAC-crosslinked non-expanding gelling solution [10.4% (w/v) acrylamide, 0.2% (w/v) BAC, 0.05% (w/v) TEMED, 0.05% (w/v) APS] for 5 min with gentle shaking. After the incubation, the non-expanding gelling solution was removed from the well, and the glass slide carrying the expanded gel was transferred to a gelation chamber. Spaces consisting of a stack of #1.5 coverslips were placed on either side of the gel, and the chamber was closed with a rectangular coverslip. The non-expanding gelling solution was added from the side of the chamber until the chamber was completely filled. The gelation chambers were incubated for 2 hours at 37 °C. After gelation, the chambers were opened by removing the top coverslip. Side lengths of the parallelogram were measured. The gels were trimmed to leave only the portion inside the parallelogram, while preserving the shape of the parallelogram. Side lengths of the trimmed gels were measured. Finally, the trimmed gels were washed twice in PBS, each time for 10 min.

1st Linker hybridization

The gels were incubated in hybridization buffer [4x SSC + 20% (v/v) formamide] for 30 min at room temperature. For readout after 2-round expansion (~10-20x expansion factor), the gels were incubated with 1 nmol of oligo 5'Ac-B1'-4xB2' in 500 µL of hybridization buffer overnight at room temperature. For readout after 3-round expansion (~40-80x expansion factor), the gels were incubated with 1 nmol of oligo 5'Ac-B1'-A2' in 500 µL of hybridization buffer overnight at room temperature. After incubation, the gels were washed in hybridization buffer three times, each time for 1 hour, and then overnight, all with gentle shaking. The gels were then washed three times in PBS, each time for 5 min.

Re-embedding into a DATD-crosslinked expanding 3rd gel

The gels were incubated in DATD-crosslinked expanding gelling solution [8.6% (w/v) sodium acrylate, 2.6% (w/v) acrylamide, 0.5% (w/v) DATD, PBS, 2M NaCl, 0.01% (w/v) 4-HT, 0.2% (w/v) TEMED, 0.2% (w/v) APS] for 30 min at 4 °C. The gels (with the virion side down) were enclosed in gelation chambers, incubated for 2 hours at 37 °C, size-measured, trimmed, size-re-measured, and washed as described in “*Re-embedding into a BAC-crosslinked non-expanding 2nd gel*”.

Cleaving BAC-crosslinked 1st and 2nd gels

The gels were incubated in BAC-cleaving buffer (0.25M TCEP-HCl, 0.75M Tris-HCl, pH 8.0) overnight at room temperature. The gels were then washed four times in PBS, each time for 30 min. For samples designated for 3-round expansion, the gels were incubated in thiol-blocking buffer (100 mM maleimide, 100 mM MOPS, pH 7.0) for 2 hours at room temperature. The thiol-blocked gels were washed three times in PBS, each time for 10 min.

LNA hybridization for readout after 2-round expansion

For samples designated for 2-round expansion, the gels were incubated with 1 nmol of LNA_B2-Atto647N in 500 µL of hybridization buffer. The LNA-hybridized gels were washed in hybridization buffer three times, each time for 1 hour, and then overnight, all with gentle shaking. The gels were then washed three times in PBS, each time for 5 min.

Gel expansion, immobilization, and imaging for 2-round expanded samples

The gels were trimmed into smaller pieces (~5 by 5 mm) while preserving the shape of the parallelogram. First, the gels were transferred (with the virion side down) into a rectangular 4-well dish that carries a glass slide in each well, and expanded in water three times, each time for 30 min. A glass-bottom 6-well plate was modified with poly-lysine, and the expanded gels were gently transferred to the poly-lysine modified coverslip surface for imaging, as previously described⁴.

Re-embedding into a DATD-crosslinked non-expanding 4th gel (for 3-round expansion)

Thiol-blocked gels in “*Cleaving BAC-crosslinked 1st and 2nd gels*” were subsequently trimmed into smaller pieces (~5 by 5 mm) while preserving the shape of the parallelogram. The gels were transferred (with the virion side down) into a rectangular 4-well dish that carries a glass slide in each well, and expanded in water three times, each time for 30 min. The gels were transferred onto a slide glass and trimmed in the z-direction into a thickness of 1 mm. Briefly, the glass slide (with 1-mm thickness) carrying the expanded sample was placed between two stacks of 1-mm-glass slides, and a cryostat blade was pushed slowly through the expanded gel. The bottom gel, which carries the virions at the bottom side, was transferred back to the 4-well plate. The z-trimmed gels were then incubated in DATD non-expanding gelling solution [10.4% (w/v) acrylamide, 0.5% (w/v) DATD, 0.05% (w/v) TEMED, 0.05% (w/v) APS] for 30 min at 4 °C. The gels were enclosed in gelation chambers, incubated for 2 hours at 37 °C, size-measured, trimmed, size-re-measured, and washed as described in “*Re-embedding into a BAC-crosslinked non-expanding 2nd gel*”.

2nd Linker hybridization

The gels were incubated in hybridization buffer [4x SSC + 20% (v/v) formamide) for 30 min at room temperature. The gels were incubated with 0.5 nmol of oligo 5’Ac-A2-4xB2’ in 1 mL of hybridization buffer overnight at room temperature. After incubation, the gels were washed in hybridization buffer three times, each time for 1 hour, and then overnight, all with gentle shaking. The gels were then washed twice in PBS, each time for 30 min.

Re-embedding into a bis-crosslinked expanding 5th gel

The gels were incubated in bis-crosslinked expanding gelling solution [8.6% (w/v) sodium acrylate, 2.6% (w/v) acrylamide, 0.15% (w/v) N,N-methylenebisacrylamide (bis), PBS, 2M NaCl, 0.01% (w/v) 4-HT, 0.2% (w/v) TEMED, 0.2% (w/v) APS] for 30 min at 4 °C. The gels (with the virion side down) were enclosed in gelation chambers, incubated for 2 hours at 37 °C, size-measured, trimmed, size-re-measured, and washed in the same way as described in “*Re-embedding into a BAC-crosslinked non-expanding 2nd gel*”.

Cleaving DATD-crosslinked 4th and 5th gels

The gels were incubated in DATD-cleaving buffer (20 mM sodium periodate, PBS, pH 5.5) for 30 min at room temperature. The gels were then washed three times in PBS, each time for 30 min, and then overnight with gentle shaking.

LNA hybridization for readout after 3-round expansion

The gels were hybridized with LNA_B1_Atto647N as described in “*LNA hybridization for readout after 2-round expansion*”.

Gel expansion, immobilization, and imaging

The gels were trimmed, expanded, immobilized and imaged as described in “*Gel expansion, immobilization, and imaging for 2-round expanded samples*”.

Expansion factor estimation

Side lengths of the gels were recorded before and after each trimming step (for example, after every re-embedding step and before every gel immobilization step) and immediately before imaging. Single-stage expansion factor was calculated by taking the averaged quotient between the pre-trimming size of the current step and the post-trimming size of the previous step. Overall expansion factor was calculated from the product of all the previous single-step expansion factors until the final step. Typical overall expansion factor for TG-based 2-round iterative expansion, for example, ranged from ~10x to ~13x for the virion expansion experiments. However, we also observed up to ~20x expansion in some experiments (e.g., HIV expansion) that were carried out towards the end of the project, when older monomer stock solutions (stored for 3 years at -80 °C) and low-quality sodium acrylate (due to the commercial supply issue) were used. We therefore recommend using freshest possible monomer solution (< 1 year) and high-quality sodium acrylate (transparent in colour and void of precipitates when dissolved) for gelation.

Expansion of HIV and VSV virions (direct labelling and iterative expansion)

Purified HIV virions and VSV virions were immobilized, fixed, conjugated with oligos, gelled, and expanded following the 2-round iterative expansion protocol of HSV-1 virions described above.

Imaging

Unless otherwise noted, all the expanded samples were imaged with an Andor spinning disk (CSU-W1, Yokogawa) confocal system on a Nikon Eclipse Ti-E microscope body with a CFI Apo LambdaS LWD 40x, 1.15 NA water-immersion objective (Nikon), controlled by NIS-Elements AR v4.60.00 (Nikon). The two-colour HeLa cell tubulin and clathrin images and all the virion images were deconvolved with theoretical point-spread functions (PSFs) (Huygens Essential for MacX11 built on Feb 7, 2013, SVI) before visualization and image analysis.

Image and data visualization

Unless otherwise noted, all the 3D renderings were generated using Imaris x64 8.3 (Oxford Instruments). Part of the image datasets were analysed and visualized using ImageJ (Fiji) 2.10/1.53c. Part of the plots were generated using OriginPro8.1 (Origin).

Peak-to-peak distance analysis of microtubule sidewalls

The peak-to-peak distance between microtubule sidewalls was measured using a semi-automated algorithm implemented on MATLAB R2018a-R2020b (“Microtubule Peak-to-Peak Distance Analysis”), which is available for download⁴⁹. Briefly, on maximum intensity z-projection

images of beta-tubulin-stained HeLa cells, two points were manually selected along the centreline of a microtubule segment. A 200 nm (in biological length) segment was then cropped out from the selected segment, to refine the selection and standardize the length of analysed segments. The line intensity profile along the 200 nm segment was fitted with two Gaussian functions to detect the two peaks in the fluorescence intensity, between which the distance was measured as the peak-to-peak distance of the microtubule sidewalls.

Single-particle averaged virion images

Single-particle averaged virion images were generated using a semi-automated image analysis pipeline implemented on MATLAB R2018a-R2020b (“Virus Particle Analysis”), which is available for download⁴⁸. First, within an acquired image z-stack, all round objects with a local minimum inside the object were identified as virions. The centre of each virion was then determined manually within the image z-plane that had the largest virion diameter. Next, the centre of the virions was re-inspected and re-aligned once more. During the second inspection, a small portion (<10%) of the virions, which had significant overlaps with neighbouring virions, were rejected from the averaging. Finally, individual virion images around each virion centre were automatically cropped, calibrated with the expansion factor, and arithmetically averaged. For display purpose, the single-particle averaged virion images were background-subtracted and brightness/contrast-adjusted.

Spatial analysis of virion envelope proteins

Spatial arrangements of the virion envelope proteins were quantified using the semi-automated image analysis pipeline implemented on MATLAB R2018a-R2020b (“Virus Particle Analysis”)⁴⁸.

All virions that passed the second inspection in the previous section were analysed using the following semi-automated procedure. For each particle, the z-plane that corresponded to the vertical centre of the particle (z-midplane) was manually identified by selecting the one with maximum contour diameter of the envelope layer. From the z-midplane image, the radii in 8 directions (45 degrees apart) were algorithmically measured by computing the distance from the particle centroid to the Gaussian-fitted centre of the envelope profile. Manual inspection was carried out to exclude portions of the 8 radii that were measured either incorrectly or with low confidence, based on the following criteria for rejection: (1) when the line intensity profile contained peaks that belonged to other virions, (2) when the envelope layer in the particular direction was not present or was significantly dimmer than that in other directions, or (3) when the automated Gaussian fitting failed. Standard deviation of all the accepted radii within the same particle (σ) was reported as population statistics for virions with ≥ 3 accepted radii. For radii normalization, the accepted radii were divided by their mean, such that the mean of all the normalized radii (R_n) was equal to 1.

For HSV-1 virion shape analysis, virions with ≥ 6 accepted radii (for eccentricity, virions with ≥ 6 accepted radii and with the accepted radii constituting at least 2 mutually perpendicular diameters to serve as the major and minor axes) were used to assure an accurate approximation of the particle shapes, and only the accepted radii within each particle were used to calculate the following shape descriptors. Eccentricity (e) was defined as the ratio of the minor axis to the

major axis (values between 0 and 1; perfect circle = 1; particles with ≥ 6 accepted radii and with the accepted radii constituting at least 2 mutually perpendicular diameters to serve as major and minor axes were used). Sphericity (s) was defined as the ratio of the radius of the inscribing circle to the radius of the circumscribing circle (values between 0 and 1; perfect circle = 1; particles with ≥ 6 accepted radii were used). Normalized circular standard deviation (σ_n) was defined as the standard deviation of R_n within each particle (values between 0 and 1; perfect circle = 0; particles with ≥ 6 accepted radii were used). We note that the exact same criteria were used to accept radii within each particle, and to select particles for the shape descriptor calculations for the TG- and PAAG-expanded virions.

Modelling and simulation of single-particle averaged HSV-1 virion images

General description of the model

A model of spherical virions was developed on MATLAB R2020a-R2020b based on experimental parameters derived from individual HSV-1 virions, in order to simulate the single-particle averaged HSV-1 virion images and their quantitative metrics (“HSV-1 Averaged Particle Image Simulation”)⁵⁰.

Model design and assumption

The model was developed based on the following design principles and assumptions. (1) We assumed that the oligo-conjugation procedure for the envelope proteins, which we experimentally applied to obtain the virion images, only labelled the envelope proteins of the virion. This assumption is based on the fact that the DNA oligo used, a highly negatively charged 22-mer, is unlikely to cross the virion membrane, and is therefore only conjugated to the exposed amine-containing species outside the membrane, namely the envelope proteins. (2) We assumed that, at the individual particle level, the fluorescence intensity profile along the line that extends from the centre of the virion towards the edge of the image (which we refer to as “radial intensity profile”) could be represented by a single Gaussian function. This assumption was made based on the following two considerations. First, the line from which we collected the radial intensity profile would only intersect the fluorescently-labelled envelope protein layer at a single point. Due to optical diffraction, the radial intensity profile of a point-source of fluorophore would be similar to a point-spread-function (PSF), whose profile can be readily approximated by a Gaussian function (as commonly used to fit single fluorescent emitters in single-molecule localization microscopy, such as PALM and STORM). Second, our experimental results indicated that the majority (> 60 -70%) of the radial intensity profiles can be fit well by a Gaussian function, as exemplified by the representative radial intensity profile in **Fig. 4f** (with the red line indicating the Gaussian fit). We note that the remaining 30-40% of the radial intensity profiles contained additional fluorescence signals from neighbouring virions or debris in the sample, and can be, in principle, approximated by sums of multiple Gaussians. To keep the model simple, we did not incorporate these additional signals in the simulation. (3) We assumed that all the radial intensity profiles collected from a given gel type had the same Gaussian spread. The width of the PSF, based on Abbe’s theorem of diffraction, is ~ 250 nm (calculated from the Abbe criterion of our imaging system), and should be constant across all the virions imaged. To be converted to a biologically relevant pre-expansion length scale, however, the PSF width needs to be normalized (by division) by the linear expansion factor. Because TG and PAAG differ in their expansion factors, the width of the PSF at the pre-expansion scale is different for each gel type. (4) We assumed that all the radial intensity profiles had the same peak fluorescence

intensity. This assumption was based on the experimental observation that, likely due to the fixed stoichiometry of the signal amplification scheme employed in the iterative expansion (in which the DNA oligos were conjugated in pre-defined ratios that are based on the oligo design; for instance, the linker oligo harboured exactly 1 binding site for the upstream oligo, and 4 binding sites for the downstream oligo), the fluorescence along the viral envelope protein layer showed approximately equal brightness. (5) We assumed that there was no orientation-specific effect for the virion samples and the resulting images throughout the experimental procedure. In other words, the expanded virions were randomly oriented when imaged.

Simulation of the single-particle averaged HSV-1 virion images based on the model

Simulation was performed at two levels: the individual particle level and the single-particle averaged image level. We first developed a simulator of the radial intensity profiles at the individual particle level. In this simulator, we started with an individual particle in a given gel type, and simulated all 8 of its radial intensity profiles, in 8 equally spaced directions (45 degrees apart). This is analogous to how we performed the radii analysis in **Fig. 4f**, but instead of extracting radial intensity profiles from an experimentally derived image, we simulated these profiles as individual Gaussian functions, based on Assumption #2 in the previous section. The Gaussian function was defined by two parameters, μ , which specifies the centre of the bell-shaped curve, and σ , which specifies its spread (or width). The μ parameter of a single radial profile represents the radius of the particle in that direction, and it must capture the effect of the variable particle size, which arises from the natural biological variability as well as the chemical variability associated with the gel type (e.g., variability in the local expansion factor). Thus, to define μ , we first selected a single value of intra-particle mean radii, out of the list of all the experimentally derived intra-particle mean radii values for particles with ≥ 3 accepted radial profiles (particles with < 3 accepted radial profiles were excluded from this list because they provided less accurate intra-particle statistics of their radii) for a given gel type ($n = 352$ values for TG and 330 values for PAAG), and then set the μ parameter of all the 8 Gaussian functions to this value, as their initial values. Besides the effect of the variable particle size, the μ parameter must also capture the variability of radii within a particle, which is predominantly caused by the local distortions introduced by the hydrogel in the expansion process. Previous cryo-ET studies have shown that the HSV-1 virion envelope is a smooth and continuous layer with only a slight departure from a spherical shape [σ_b (σ from the naturally occurring biological variability) = ~ 2.6 nm; estimated from previously characterized aspect ratios of virions⁴², see below]. Notably, the difference between this biological variability and the experimentally-derived median of the intra-particle standard deviation of radii amounts to $\sigma_c = \sim 8.8$ nm [= sqrt($9.2 \text{ nm}^2 - \sigma_b^2$)] for TG and $\sigma_c = \sim 14.0$ nm [= sqrt($14.3 \text{ nm}^2 - \sigma_b^2$)] for PAAG, suggesting that nearly all of the intra-particle variability of the radii came from the expansion process. To incorporate this effect, within a given particle, we displaced the 8 μ parameters either by adding (performed on a random 4 out of the 8 μ values) or subtracting (performed on the other 4 μ values) the experimentally-derived median of the intra-particle standard deviation of radii [$\sigma_m = 9.2$ nm (TG) and 14.3 nm (PAAG); see **Fig. 4g**]. This method of displacement preserved the mean intra-particle radii, while equating the intra-particle standard deviation of radii, in the to-be-simulated particle, to the median value derived from the experimental data.

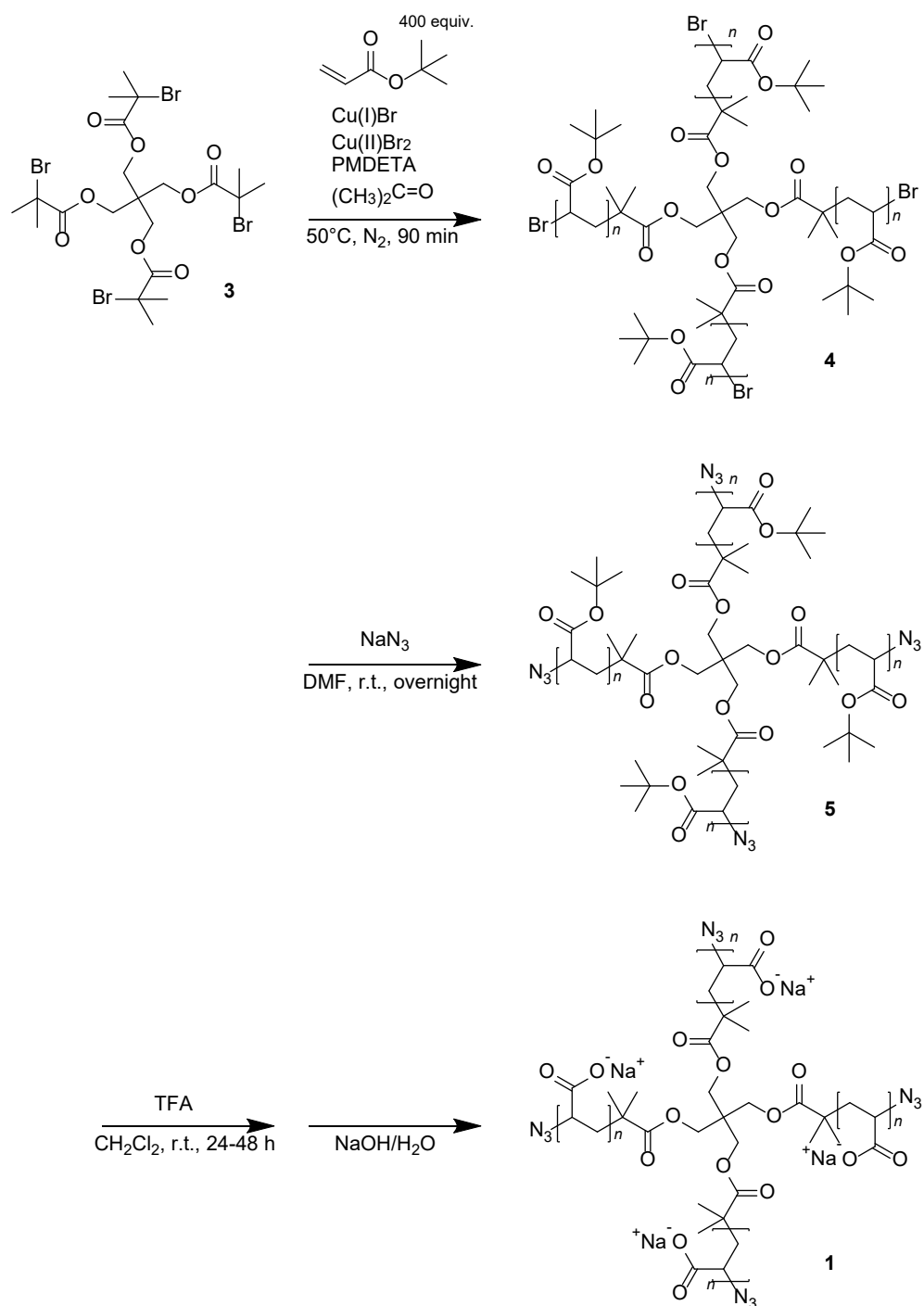
Next, to define σ , we used the median value of all the experimentally-derived σ parameters, which we collected from Gaussian fittings of all the radial intensity profiles in a

given gel type [20.8 nm (median) for TG and 15.3 nm (median) for PAAG; 1977 (TG) profiles across 352 virions from a single batch of live HSV-1 preparation, and 1889 (PAAG) profiles across 330 virions from a single batch of live HSV-1 preparation, same batch as TG], based on Assumption #3. With these parameters, we generated 8 Gaussian distributions for the 8 radial intensity profiles, for a given particle. Next, we repeated this simulation n times, where n is the sample size for the experimental single-particle averaged images [$n = 396$ (TG) and 362 (PAAG)], in order to include the same level of averaging effect to the to-be-simulated averaged image. We averaged n sets of the 8 particle-level radial intensity profiles within each of the 8 directions, to generate a single set of 8 radial intensity profiles at the single-particle averaged image level. Thus, these 8 radial intensity profiles were the simulated counterparts of the 8 radial intensity profiles collected from the experimentally-derived averaged images. We used the same analytical procedure, as applied to the experimental images, to extract the quantitative metrics from these simulated radial intensity profiles, which included the intra-particle standard deviation of radii (σ_a), and the median full-width-half-maximum (FWHM) of the 8 radial intensity profiles. To facilitate visualization of the simulated radial intensity profiles at the single-particle averaged image level (and not for quantitative analysis; all quantitative analysis was performed on the 8 simulated radial intensity profiles), we used a representative simulated radial intensity profile to model the full averaged image with the following procedure. First, we observed that the 8 simulated averaged radial intensity profiles were nearly identical to one another, which is based on the observation that at any given radial position (i.e., at any given x -value of the radial intensity profile), the standard deviation of the 8 intensity values (the corresponding y -values), collected from the 8 averaged profiles at that position, are constantly less than $\sim 5\%$ of their mean value. We then simulated the full image using a single representative averaged profile, which substantially simplified the construction of the simulated full image. We selected a representative radial intensity profile with FWHM closest to the median of the 8 profiles. We then generated an array of pixels with the same pixel size as the experimental single-particle averaged images, and assigned fluorescence intensity to each pixel by calculating the distance of the pixel from the centre of the image (which corresponded to the centroid of the particle), and assigning the intensity value at this distance from the representative radial intensity profile.

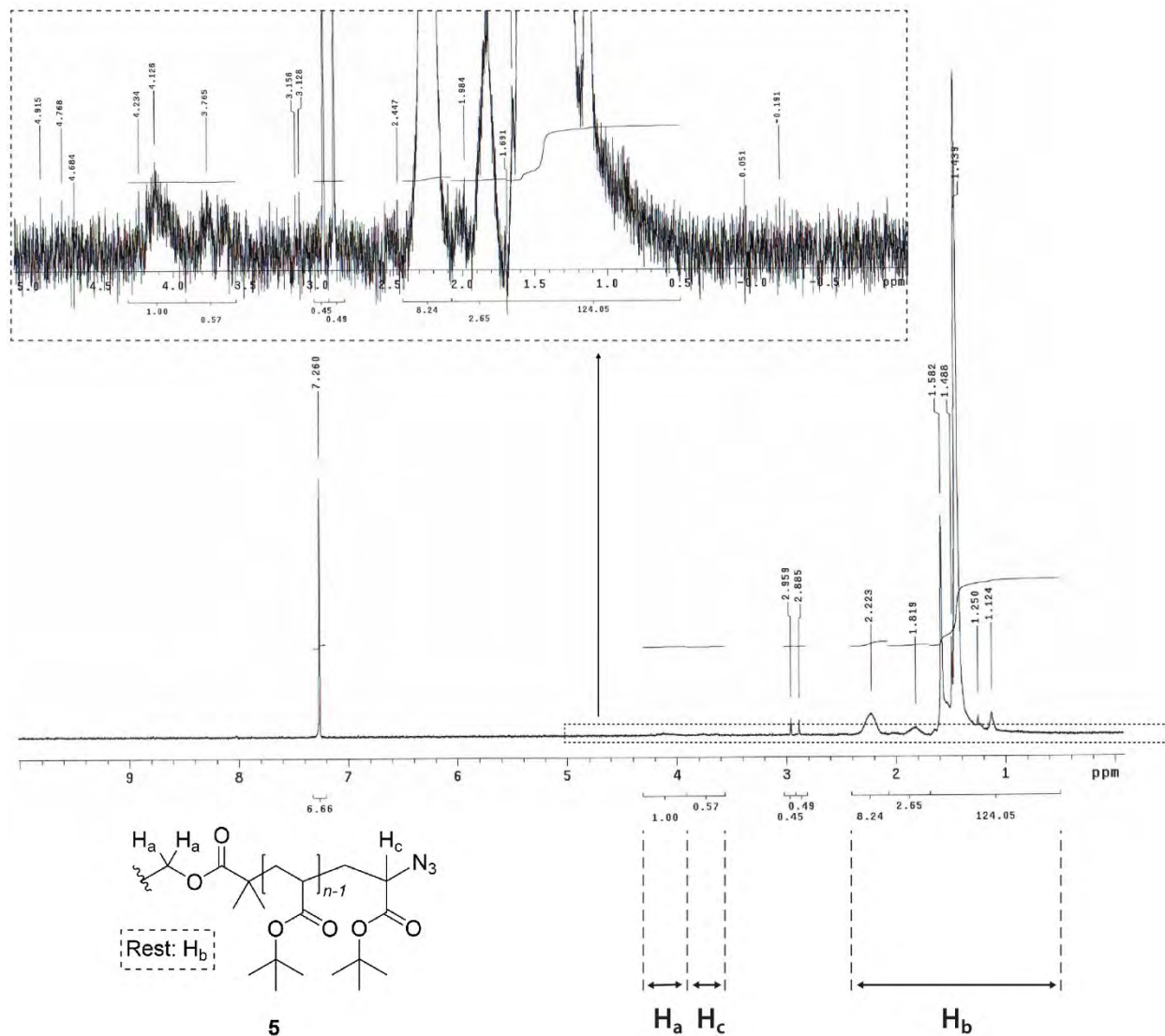
Estimation of ground-truth deviation of HSV-1 virions from spherical shapes (σ_b)

To estimate the deviation from spherical shapes for ground-truth HSV-1 virions based on cryo-ET imaging, their shapes were modelled as ellipses, whose aspect ratios were set equal to the representative aspect ratio previously characterized by a cryo-ET study⁴². The representative aspect ratio, 1.07, was determined by estimating the median of all the reported values in the study. To derive σ_b from a simulated ellipse, we performed the same analysis as applied to our experimentally-derived HSV-1 virions, by measuring its radii in 8 directions that were equally spaced apart. We repeated this procedure for 10,000 individual simulated ellipses with each rotated by a random angle, and used the median value (~ 2.6 nm) of the population as σ_b for the HSV-1 virions.

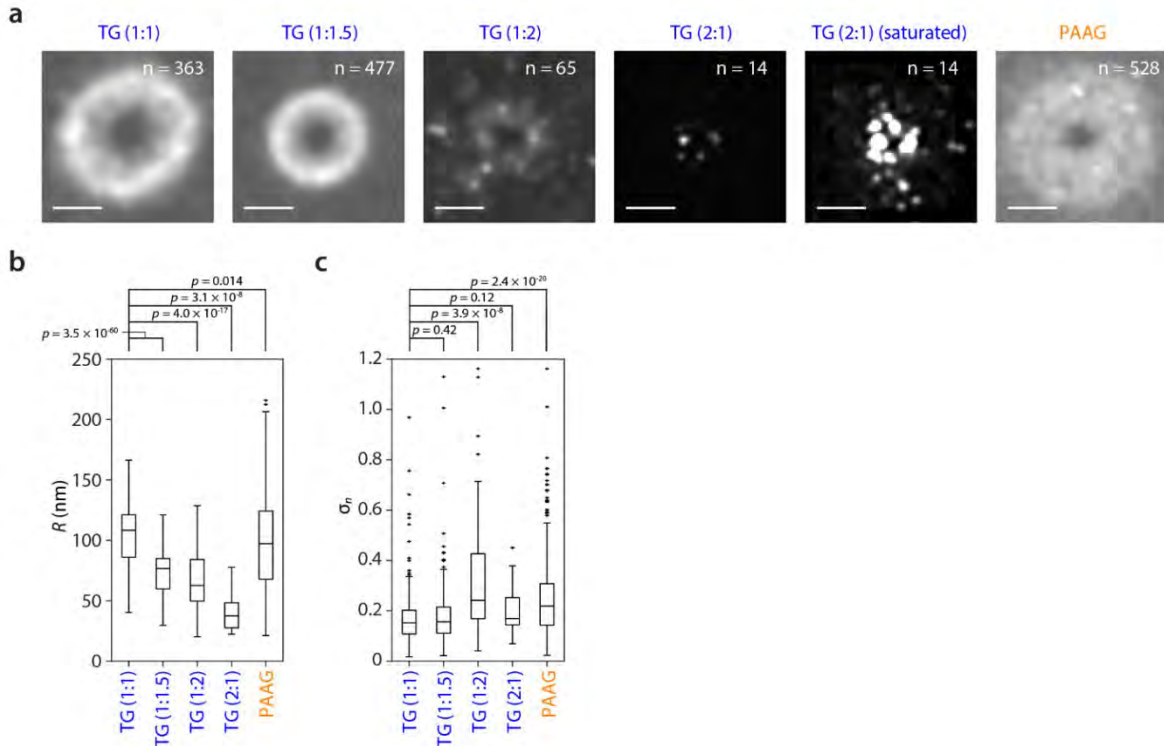
Supplementary Figures and Tables



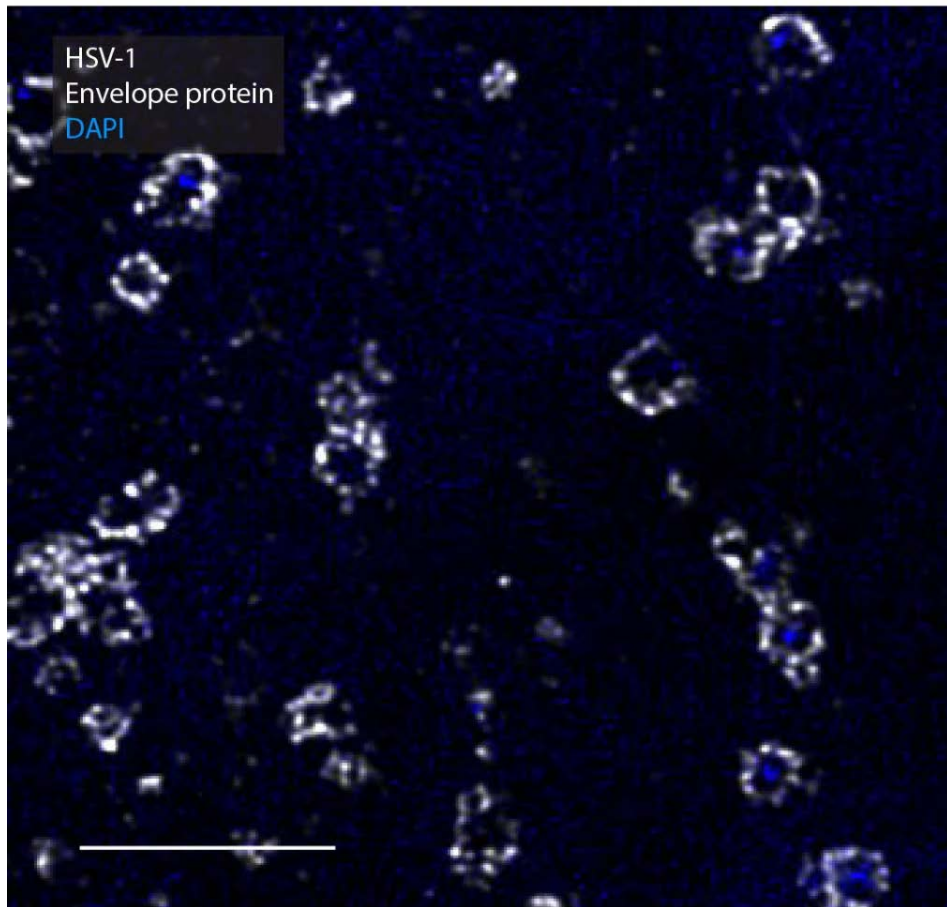
Supplementary Fig. 1. Synthesis of monomer 1.



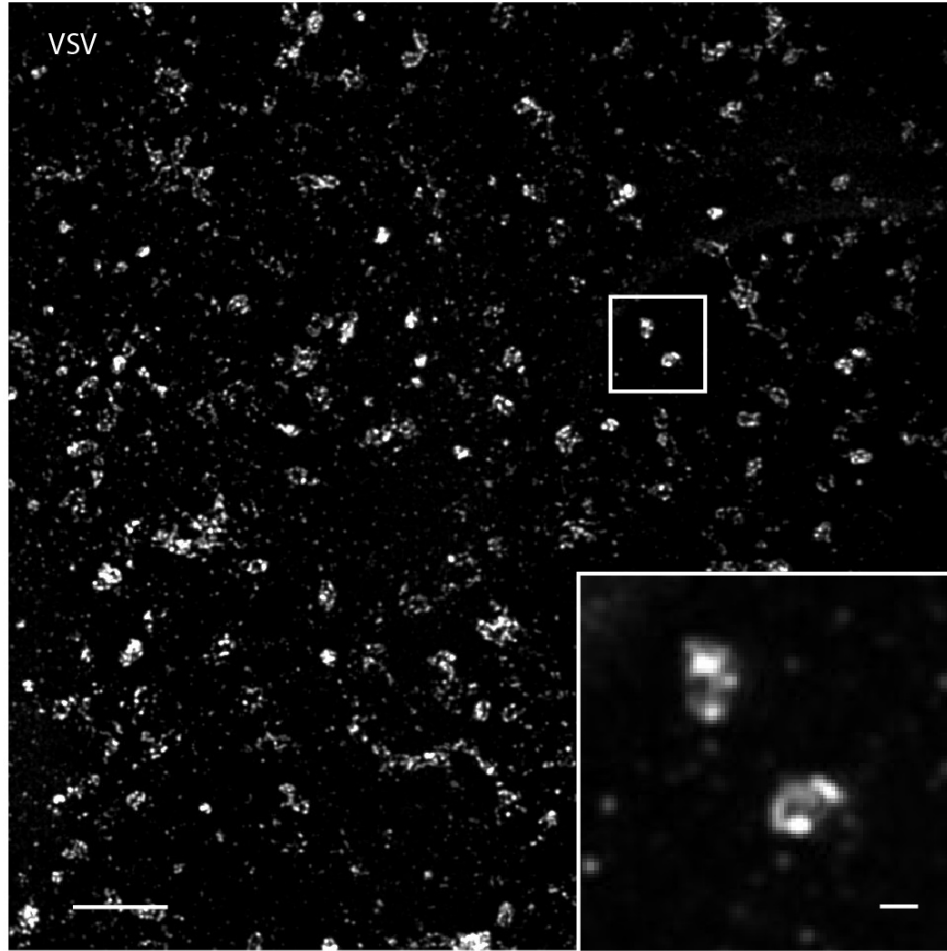
Supplementary Fig. 2. ¹H NMR spectra of tetra-arm poly(t-butyl acrylate) with azide terminal groups (**5**) in chloroform-d. H_a, H_c, and H_b indicate the core, end, and backbone H, respectively.



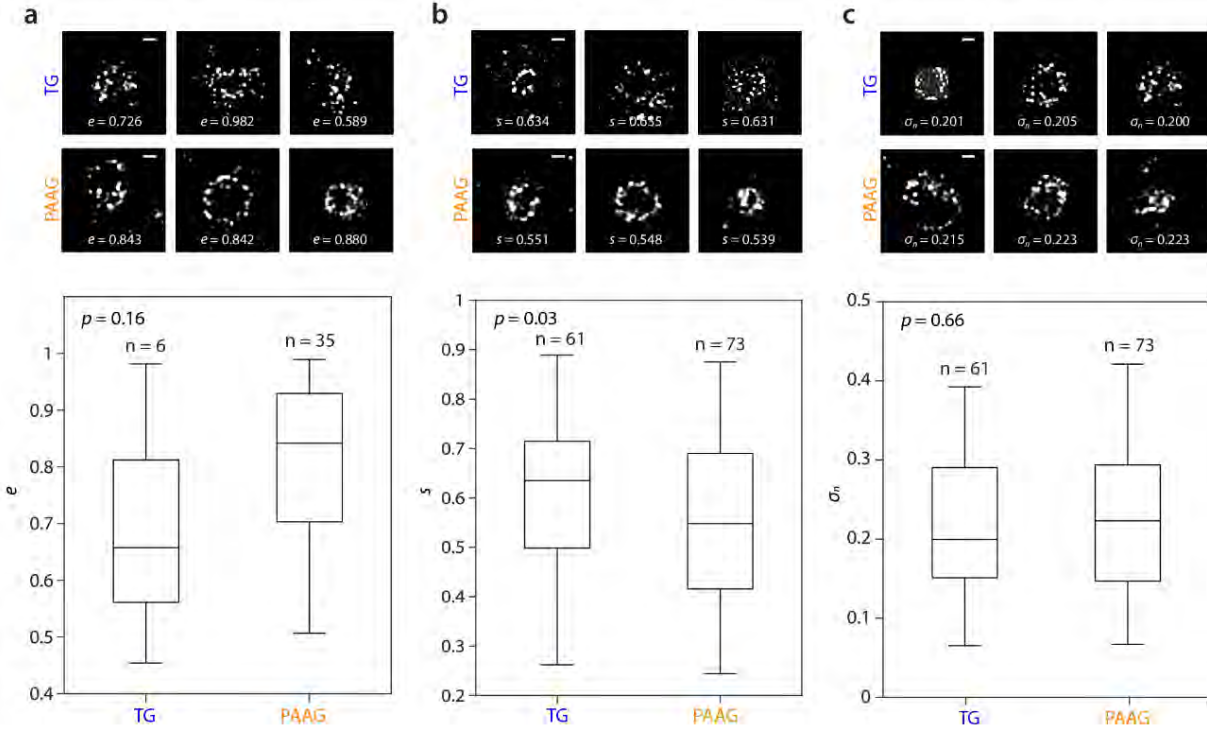
Supplementary Fig. 3. Off-the-ratio tetra-gel (TG) and expansion. **a**, Single-particle averaged images of herpes simplex virus type 1 (HSV-1) virions expanded by TG (1:1), TG (1:1.5), TG (1:2), TG (2:1), TG (2:1) (the same image saturated to show the virion contours), and PAAG-based 2-round iterative expansion [TG (1:1), $n = 363$; TG (1:1.5), $n = 477$; TG (1:2), $n = 65$; TG (2:1), $n = 14$; PAAG, $n = 528$ virions; virions from the same single batch of live HSV-1 preparation]. The ratios in the brackets indicate molar ratios of monomer 1 to monomer 2 for TG. Scale bars, 100 nm. **b**, HSV-1 virion radii (R) for TG (1:1), TG (1:1.5), TG (1:2), TG (2:1), and PAAG-based 2-round iterative expansion [$p = 3.5 \times 10^{-60}$ for TG (1:1) and TG (1:1.5), 4.0×10^{-17} for TG (1:1) and TG (1:2), 3.1×10^{-8} for TG (1:1) and TG (2:1), 0.014 for TG (1:1) and PAAG, 2-sided Wilcoxon rank sum test; TG (1:1), $n = 360$; TG (1:1.5), $n = 465$; TG (1:2), $n = 56$; TG (2:1), $n = 12$; PAAG, $n = 512$ virions; virions from the same single batch of live HSV-1 preparation]. **c**, Normalized circular standard deviation (σ_n) of HSV-1 virion z-midplane cross-sections for TG (1:1), TG (1:1.5), TG (1:2), TG (2:1), and PAAG-based 2-round iterative expansion [$p = 0.42$ for TG (1:1) and TG (1:1.5), 3.9×10^{-8} for TG (1:1) and TG (1:2), 0.12 for TG (1:1) and TG (2:1), 2.4×10^{-20} for TG (1:1) and PAAG, 2-sided Wilcoxon rank sum test; TG (1:1), $n = 360$; TG (1:1.5), $n = 465$; TG (1:2), $n = 56$; TG (2:1), $n = 12$; PAAG, $n = 512$ virions; virions from the same single batch of live HSV-1 preparation]. HSV-1 radii are, as noted in the main text, identified using cryo-EM to have radii of ~ 90 nm. In **b-c**, data are presented as box plots with ends of whiskers representing maximum and minimum values of the distribution after outlying points (values above 75th percentile + $1.5 \times$ interquartile range, or below 25th percentile - $1.5 \times$ interquartile range) are excluded, upper line of box representing 75th percentile, middle line of box representing 50th percentile (median), lower line of box representing 25th percentile, and plus signs representing individual values for the outlying points.



Supplementary Fig. 4. Two-colour imaging of HSV-1 virion envelope proteins (white) and DNA (blue). The virions were expanded by TG-based 2-round iterative expansion with direct labelling of the envelope proteins. Expansion factor, 10.7x. Scale bar, 1 μm (10.7 μm). Results are representative of 5 separately acquired fields of view from a single hydrogel preparation, using virions from the same single batch of live HSV-1 preparation.

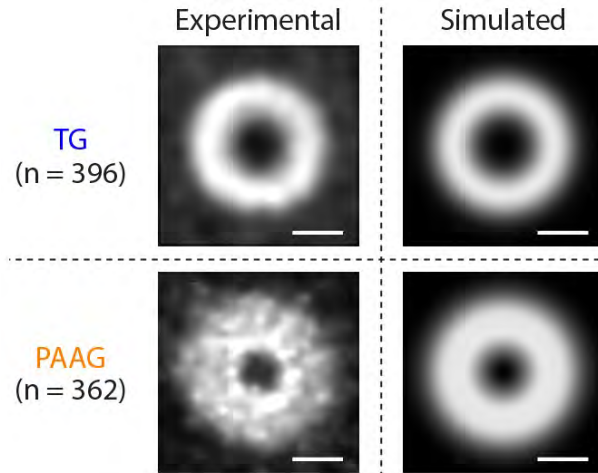


Supplementary Fig. 5. Expansion of vesicular stomatitis virus (VSV) virions. The VSV virions were expanded by TG-based 2-round iterative expansion with direct labelling of the envelope proteins. Expansion factor, 10.9x. Scale bar, 1 μm (10.9 μm). Inset, magnified view of the boxed region on a single xy-plane. Scale bar, 100 nm (1.09 μm). Results are representative of 3 separately acquired fields of view from a single hydrogel preparation, using virions from the same single batch of live VSV preparation.



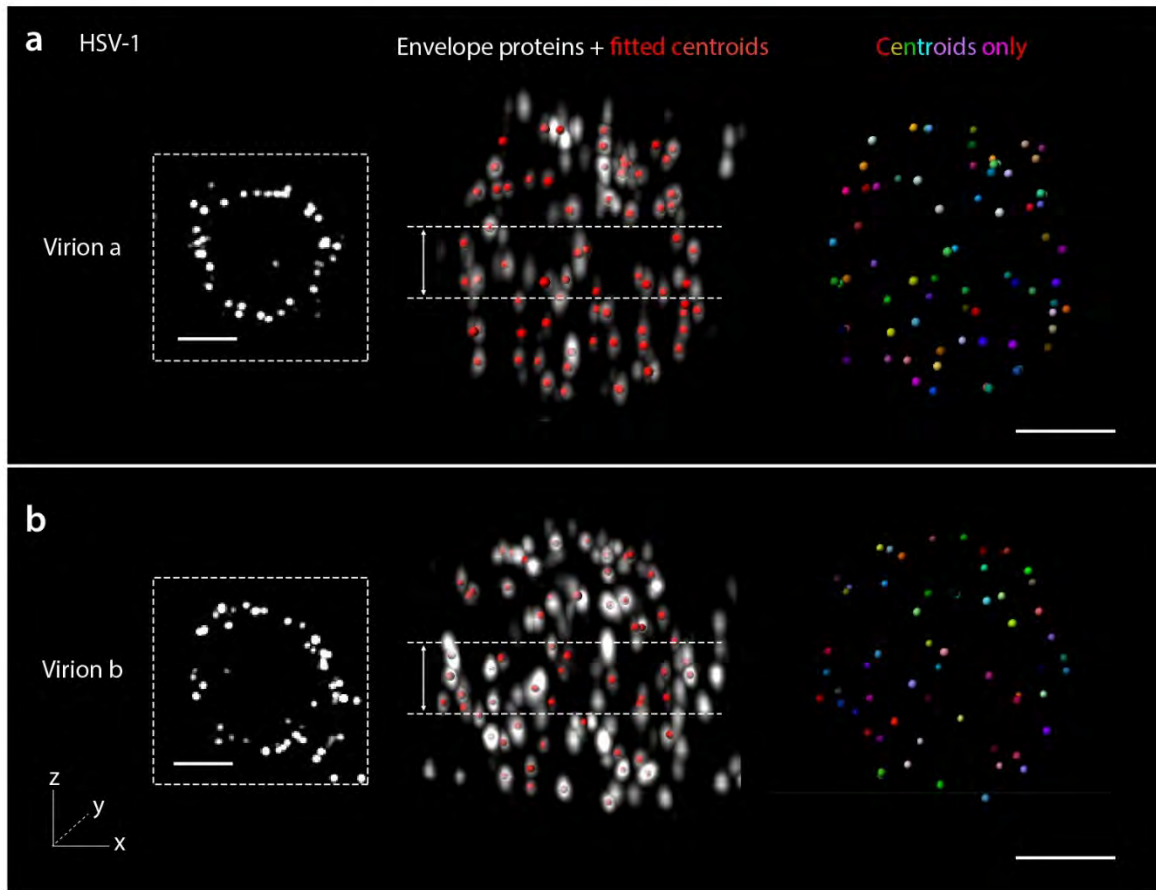
Supplementary Fig. 6. Expansion of human immunodeficiency virus (HIV) virions. **a.** Top, HIV virions expanded by TG- (top row) and PAAG-based (bottom row) 2-round iterative expansion, with the z-midplane cross-sectional shapes scoring close to the median value of eccentricity (e) within each hydrogel group. Bottom, eccentricity (e) of HIV virion z-midplane cross-sections for TG- and PAAG-based iterative expansion ($p = 0.16$, 2-sided Wilcoxon rank sum test; TG, $n = 6$; PAAG, $n = 35$ virions; virions from the same single batch of live HIV preparation). Scale bars, 100 nm. **b.** Top, HIV virions expanded by TG- (top row) and PAAG-based (bottom row) 2-round iterative expansion, with the z-midplane cross-sectional shapes scoring close to the median value of sphericity (s) within each hydrogel group. Bottom, sphericity (s) of HSV-1 virion z-midplane cross-sections for TG- and PAAG-based iterative expansion ($p = 0.03$, 2-sided Wilcoxon rank sum test; TG, $n = 61$; PAAG, $n = 73$ virions; virions from the same single batch of live HIV preparation). Scale bars, 100 nm. **c.** Top, HIV virions expanded by TG- (top row) and PAAG-based (bottom row) 2-round iterative expansion, with the z-midplane cross-sectional shapes scoring close to the median value of normalized circular standard deviation (σ_n) within each hydrogel group. Bottom, normalized circular standard deviation (σ_n) of HIV virion z-midplane cross-sections for TG- and PAAG-based iterative expansion ($p = 0.66$, 2-sided Wilcoxon rank sum test; TG, $n = 61$; PAAG, $n = 73$ virions; virions from the same single batch of live HIV preparation). Scale bars, 100 nm. In **a-c**, data are presented as box plots with ends of whiskers representing maximum and minimum values of the distribution after outlying points (values above 75th percentile + $1.5 \times$ interquartile range, or below 25th percentile - $1.5 \times$ interquartile range) are excluded, upper line of box representing 75th percentile, middle line of box representing 50th percentile (median), lower line of box representing 25th percentile, and plus signs representing individual values for the outlying points. For HIV virion shape analysis, virions with ≥ 3 accepted radii (for eccentricity, virions with \geq

4 accepted radii and with the accepted radii constituting at least 2 mutually perpendicular diameters to serve as major and minor axes) were used, and only the accepted radii within each particle were used to calculate the shape descriptors. One descriptor (s) showed significantly smaller median deviation from a perfect circle for TG, than for PAAG. The other two descriptors (e and σ_n) did not show statistically significant differences, perhaps due to small numbers of viral particles expanded, as a result of low chemical supplies, and poor yields for image processing due to sparse viral boundary labelling.



Supplementary Fig. 7. Simulation of single-particle averaged HSV-1 virion images.

Experimental (left) and simulated (right) single-particle averaged images of HSV-1 virions after TG (top)- and PAAG-based (bottom) 2-round iterative expansion (TG, $n = 396$; PAAG, $n = 362$ virions; virions from the same single batch of live HSV-1 preparation for the experimental images). Full width half maximum (FWHM) of the radial intensity profile, 73.6 nm (TG, experimental), 91.0 nm (PAAG, experimental), 78.2 nm (TG, simulated), and 108.6 nm (PAAG, simulated). Standard deviation of the radii (σ_a), 3.4 nm (TG, experimental), 4.0 nm (PAAG, experimental), 0.6 nm (TG, simulated), and 1.2 nm (PAAG, simulated). Scale bars, 100 nm.



Supplementary Fig. 8. 3D rendered images of envelope proteins of two HSV-1 virions expanded by TG-based 3-round iterative expansion. Overlay images of the deconvolved puncta (white) and the fitted centroids (red) are shown on the left, and the extracted centroids (coloured) are shown on the right. Expansion factor, 38.8x (virion a) and 38.3x (virion b). Scale bars, 100 nm (virion a, 3.88 μm ; virion b, 3.83 μm). Insets (dotted boxes), maximum intensity z-projection (MIP) of the same virions over a ~ 65 nm range around the particle centre (between the dotted lines in the 3D rendered images). Scale bars, 100 nm (virion a, 3.88 μm ; virion b, 3.83 μm).

Supplementary Table 1. DNA oligo sequences.

| Oligo Name | Purpose | Sequence (IDT format) | Modification |
|---|---|---|---------------------------------|
| For iterative expansion of HeLa cells (Fig. 3) | | | |
| 5' Amine-B1' | Conjugation to secondary antibody for pre-G1 immunostaining | AAT ACG CCC TAA GAA TCC GAA C | 5' Amino Modifier C6 |
| 5' Amine-A2' | Conjugation to secondary antibody for pre-G1 immunostaining | AAG GTG ACA GGC ATC TCA ATC T | 5' Amino Modifier C6 |
| 5' Azide-B1 | Pre-G1 adaptor for TG-based iExM | GTT CGG ATT CTT AGG GCG TA | 5' Azide |
| 5' Azide-A2 | Pre-G1 adaptor for TG-based iExM | AGA TTG AGA TGC CTG TCA CC | 5' Azide |
| 5' Acrydite-B1'-4xB2' | Post-G2 linker | TAC GCC CTA AGA ATC CGA ACA TGC ATT ACA GCC CTC AAT GCA TTA CAG CCC TCA ATG CAT TAC AGC CCT CAA TGC ATT ACA GCC CTC A | 5' Acrydite |
| 5' Acrydite-A2'-4xA1' | Post-G2 linker | GGT GAC AGG CAT CTC AAT CTA TTA CAA AGC ATC AAC GAT TAC AAA GCA TCA ACG ATT ACA AAG CAT CAA CGA TTA CAA AGC ATC AAC G | 5' Acrydite |
| LNA_B2-Atto647N | Post-G3 readout | TGAGGGCTGTAATGC | 3' Atto 647N, LNAs (underlined) |
| LNA_A1-Atto565 | Post-G3 readout | CGTTGATGCTTTGTA | 3' Atto 565, LNAs (underlined) |
| For iterative expansion of HSV-1 virions (Fig. 4) | | | |
| 5' Amine-B1' | Pre-G1 conjugation to envelope proteins | AAT ACG CCC TAA GAA TCC GAA C | 5' Amino Modifier C6 |
| 5' Acrydite-B1 | Pre-G1 adaptor for PAAG-based iExM | GTT CGG ATT CTT AGG GCG TA | 5' Acrydite |
| 3' Azide-B1 | Pre-G1 adaptor for TG-based iExM of virions | GTT CGG ATT CTT AGG GCG TA | 3' Azide |
| 5' Acrydite-B1'-4xB2' | Post-G2 linker for 2-round iExM | TAC GCC CTA AGA ATC CGA ACA TGC ATT ACA GCC CTC AAT GCA TTA CAG CCC TCA ATG CAT TAC AGC CCT CAA TGC ATT ACA GCC CTC A | 5' Acrydite |

| | | | |
|---------------------|---------------------------------|---|---------------------------------------|
| 5'Acrydite-B1'-A2' | Post-G2 linker for 3-round iExM | TAC GCC CTA AGA ATC CGA ACA TGG TGA CAG GCA TCT CAA TCT | 5' Acrydite |
| 5'Acrydite-A2-4xB2' | Post-G4 linker for 3-round iExM | AGA TTG AGA TGC CTG TCA CCA TGC ATT ACA GCC CTC AAT GCA TTA CAG CCC TCA ATG CAT TAC AGC CCT CAA TGC ATT ACA GCC CTC A | 5' Acrydite |
| LNA_B2-Atto647N | Post-G3 or Post-G5 readout | TGAGGGCTGTAATGC | 3' Atto 647N, LNAs (underlined) |

Supplementary Table 2. Recipes of hydrogel gelling solutions.

| Gel Name | Purpose | Recipe (w/v, unless otherwise noted) | | | | |
|--|---|--|-----------------------------|--------------|-----|------|
| Tetra-gel (TG) | | | | | | |
| | | Monomer 2', 2'', or 2''' (200 mg/mL DMSO) | Monomer 1 (200 mg/mL) | Water | | |
| Non-cleavable TG (Monomer 2' or 2'') | Single-round expansion | 1 part (2' or 2'') | 1 part | 4 parts | | |
| Cleavable TG (Monomer 2''') | 1 st Gel for TG-based iExM | 2 parts (2''') | 1 part | 3 parts | | |
| Sodium polyacrylate/polyacrylamide gel (PAAG) | | | | | | |
| | | Acrylamide | Sodium acrylate | Crosslinker | PBS | NaCl |
| BAC-crosslinked expanding gel | 1 st Gel for PAAG-based iExM | 2.6% | 8.6% | 0.2% BAC | 1x | 2M |
| Re-embedding gels (for TG and PAAG-based iExM) | | | | | | |
| BAC-crosslinked non-expanding gel | 2 nd Gel | 10.4% | 0 | 0.2% BAC | 0 | 0 |
| DATD-crosslinked expanding gel | 3 rd Gel | 2.6% | 8.6% | 0.5% DATD | 1x | 2M |
| DATD-crosslinked non-expanding gel | 4 th Gel | 10.4% | 0 | 0.5% DATD | 0 | 0 |
| Bis-crosslinked expanding gel | 5 th Gel | 2.6% | 8.6% | 0.15% bis | 1x | 2M |

Supplementary Table 3. Additional gelling conditions tested.

| Monomer Design | Gelling Recipe (w/v, unless otherwise noted) | | | Purpose | Results | Comments |
|---|--|-------------------------------|------------------|--|-------------------------------------|--|
| Standard monomer 2'' and monomer 1 | Monomer 2'' (250 mg/mL DMSO) | Monomer 1 (200 mg/mL) | Water | | | |
| | 1.6 parts | 1 part | 3.4 parts | Non-stoichiometric polymerization (monomer 1:monomer 2'' = 1:2) | Gel formed; expansion factor = 3.23 | Expansion factor increases when the molar ratio between monomer 1 and 2'' deviates significantly from the stoichiometric amount. |
| | 0.8 parts | 1 part | 4.2 parts | Stoichiometric polymerization (control; monomer 1:monomer 2'' = 1:1) | Gel formed; expansion factor = 2.95 | |
| | 0.6 parts | 1 part | 4.4 parts | Non-stoichiometric polymerization (monomer 1:monomer 2'' = 1:0.75) | Gel formed; expansion factor = 2.94 | |
| | 0.4 parts | 1 part | 4.6 parts | Non-stoichiometric polymerization (monomer 1:monomer 2'' = 1:0.5) | Gel formed; expansion factor = 3.58 | |
| ~2 kDa monomer 2' and standard monomer 1 | ~2 kDa Monomer 2' (100 mg/mL DMSO, 0.4 parts) | Monomer 1 (200 mg/mL), 1 part | Water, 4.6 parts | Monomer 2' with smaller MW | Opaque solution; no gelation | |
| ~2 kDa monomer 2'' and standard monomer 1 | ~2 kDa Monomer 2'' (100 mg/mL DMSO, 0.4 parts) | Monomer 1 (200 mg/mL), 1 part | Water, 4.6 parts | Monomer 2'' with smaller MW | Opaque solution; no gelation | Potential cause: insolubility of ~2 kDa monomer 2'' due to hydrophobicity of the alkyne moiety. |

| | | | | | | |
|---|---|--------------------------------------|------------------|-------------------------------------|------------------------------|--|
| ~2 kDa monomer 2''' and standard monomer 1 | ~2 kDa Monomer 2''' (100 mg/mL DMSO, 0.4 parts | Monomer 1 (200 mg/mL), 1 part | Water, 4.6 parts | Monomer 2''' with smaller MW | Opaque solution; no gelation | Potential cause: insolubility of ~2 kDa monomer 2''' due to hydrophobicity of the alkyne moiety. |
| ~10 kDa monomer 2''' and standard monomer 1 | ~10 kDa Monomer 2''' (100 mg/mL DMSO, 2 parts | Monomer 1 (200 mg/mL), 1 part | Water, 3 parts | Monomer 2''' with smaller MW | Opaque solution; no gelation | Potential cause: insolubility of ~10 kDa monomer 2''' due to hydrophobicity of the alkyne moiety. |

References

1. Chen, F., Tillberg, P. W. & Boyden, E. S. Expansion microscopy. *Science* **347**, 543–548 (2015).
2. Gao, R., Asano, S. M. & Boyden, E. S. Q&A: expansion microscopy. *BMC Biol.* **15**, 50 (2017).
3. Wassie, A. T., Zhao, Y. & Boyden, E. S. Expansion microscopy: principles and uses in biological research. *Nat. Methods* **16**, 33–41 (2019).
4. Asano, S. M. et al. Expansion microscopy: protocols for imaging proteins and RNA in cells and tissues. *Curr. Protoc. Cell Biol.* **80**, e56 (2018).
5. Hafner, A. S., Donlin-Asp, P. G., Leitch, B., Herzog, E. & Schuman, E. M. Local protein synthesis is a ubiquitous feature of neuronal pre- and postsynaptic compartments. *Science* **364**, eaau3644 (2019).
6. Schlichting, M. et al. Light-mediated circuit switching in the *Drosophila* neuronal clock network. *Curr. Biol.* **29**, 3266–3276.e3 (2019).
7. Zhao, Y. et al. Nanoscale imaging of clinical specimens using pathology-optimized expansion microscopy. *Nat. Biotechnol.* **35**, 757–764 (2017).
8. Tillberg, P. W. et al. Protein-retention expansion microscopy of cells and tissues labeled using standard fluorescent proteins and antibodies. *Nat. Biotechnol.* **34**, 987–992 (2016).
9. Chozinski, T. J. et al. Expansion microscopy with conventional antibodies and fluorescent proteins. *Nat. Methods* **13**, 485–488 (2016).
10. Chen, F. et al. Nanoscale imaging of RNA with expansion microscopy. *Nat. Methods* **13**, 679–684 (2016).
11. Ku, T. et al. Multiplexed and scalable super-resolution imaging of three-dimensional protein localization in size-adjustable tissues. *Nat. Biotechnol.* **34**, 973–981 (2016).
12. Gambarotto, D. et al. Imaging cellular ultrastructures using expansion microscopy (U-ExM). *Nat. Methods* **16**, 71–74 (2019).
13. Gao, R. et al. Cortical column and whole-brain imaging with molecular contrast and nanoscale resolution. *Science* **363**, eaau8302 (2019).
14. Chang, J.-B. et al. Iterative expansion microscopy. *Nat. Methods* **14**, 593–599 (2017).
15. Truckenbrodt, S. et al. X10 expansion microscopy enables 25 nm resolution on conventional microscopes. *EMBO Rep.* **19**, e45836 (2018).
16. Cohen, Y., Ramon, O., Kopelman, I. J. & Mizrahi, S. Characterization of inhomogeneous polyacrylamide hydrogels. *J. Polym. Sci. B Polym. Phys.* **30**, 1055–1067 (1992).
17. Yazici, I. & Okay, O. Spatial inhomogeneity in poly(acrylic acid) hydrogels. *Polymer* **46**, 2595–2602 (2005).
18. Orakdogan, N. & Okay, O. Correlation between crosslinking efficiency and spatial inhomogeneity in poly(acrylamide) hydrogels. *Polym. Bull.* **57**, 631–641 (2006).
19. Di Lorenzo, F. & Seiffert, S. Nanostructural heterogeneity in polymer networks and gels. *Polym. Chem.* **6**, 5515–5528 (2015).
20. Gu, Y., Zhao, J. & Johnson, J. A. A (macro)molecular-level understanding of polymer network topology. *Trends Chem.* **1**, 318–334 (2019).

21. Martens, P. & Anseth, K. S. Characterization of hydrogels formed from acrylate modified poly(vinyl alcohol) macromers. *Polymer* **41**, 7715–7722 (2000).
22. Lutolf, M. P. & Hubbell, J. A. Synthesis and physicochemical characterization of end-linked poly(ethylene glycol)-co-peptide hydrogels formed by Michael-type addition. *Biomacromolecules* **4**, 713–722 (2003).
23. Malkoch, M. et al. Synthesis of well-defined hydrogel networks using Click chemistry. *Chem. Commun.* 2774–2776 (2006).
24. Sakai, T. et al. Design and fabrication of a high-strength hydrogel with ideally homogeneous network structure from tetrahedron-like macromonomers. *Macromolecules* **41**, 5379–5384 (2008).
25. Fairbanks, B. D. et al. A versatile synthetic extracellular matrix mimic via thiol-norbornene photopolymerization. *Adv. Mater.* **21**, 5005–5010 (2009).
26. Cui, J. et al. Synthetically simple, highly resilient hydrogels. *Biomacromolecules* **13**, 584–588 (2012).
27. Saffer, E. M. et al. SANS study of highly resilient poly(ethylene glycol) hydrogels. *Soft Matter* **10**, 1905–1916 (2014).
28. Matsunaga, T., Sakai, T., Akagi, Y., Chung, U.-i. & Shibayama, M. Structure characterization of Tetra-PEG gel by small-angle neutron scattering. *Macromolecules* **42**, 1344–1351 (2009).
29. Matsunaga, T., Sakai, T., Akagi, Y., Chung, U.-i. & Shibayama, M. SANS and SLS studies on tetra-arm PEG gels in as-prepared and swollen states. *Macromolecules* **42**, 6245–6252 (2009).
30. Oshima, K., Fujimoto, T., Minami, E. & Mitsukami, Y. Model polyelectrolyte gels synthesized by end-linking of tetra-arm polymers with click chemistry: synthesis and mechanical properties. *Macromolecules* **47**, 7573–7580 (2014).
31. Kamata, H., Akagi, Y., Kayasuga-Kariya, Y., Chung, U.-i. & Sakai, T. “Nonswellable” hydrogel without mechanical hysteresis. *Science* **343**, 873–875 (2014).
32. Tricot, M. Comparison of experimental and theoretical persistence length of some polyelectrolytes at various ionic strengths. *Macromolecules* **17**, 1698–1704 (1984).
33. Kienberger, F. et al. Static and dynamical properties of single poly(ethylene glycol) molecules investigated by force spectroscopy. *Single Mol.* **1**, 123–128 (2000).
34. Kuhn, W. Über die Gestalt fadenförmiger Moleküle in Lösungen. *Kolloid Z.* **68**, 2–15 (1934).
35. Kuhn, W. & Kuhn, H. Die Frage nach der Aufrollung von Fadenmolekeln in strömenden Lösungen. *Helv. Chim. Acta* **26**, 1394–1465 (1943).
36. Debye, P. & Hückel, E. The theory of electrolytes. I. Lowering of freezing point and related phenomena. *Phys. Z.* **24**, 185–206 (1923).
37. Dommerholt, J., Rutjes, F. P. J. T. & van Delft, F. L. Strain-promoted 1,3-dipolar cycloaddition of cycloalkynes and organic azides. *Top. Curr. Chem.* **374**, 16 (2016).
38. Zander, Z. K., Hua, G., Wiener, C. G., Vogt, B. D. & Becker, M. L. Control of mesh size and modulus by kinetically dependent cross-linking in hydrogels. *Adv. Mater.* **27**, 6283–6288 (2015).

39. Hughes, M. P., Morgan, H. & Rixon, F. J. Dielectrophoretic manipulation and characterization of herpes simplex virus-1 capsids. *Eur. Biophys. J.* **30**, 268–272 (2001).
40. Liu, F. & Zhou, Z. H. in *Human Herpesviruses: Biology, Therapy, and Immunoprophylaxis* (eds Arvin, A. et al.) 27–43 (Cambridge Univ. Press, 2007).
41. Brown, J. C. & Newcomb, W. W. Herpesvirus capsid assembly: Insights from structural analysis. *Curr. Opin. Virol.* **1**, 142–149 (2011).
42. Grünewald, K. et al. Three-dimensional structure of herpes simplex virus from cryo-electron tomography. *Science* **302**, 1396–1398 (2003).
43. Maurer, U. E., Sodeik, B. & Grünewald, K. Native 3D intermediates of membrane fusion in herpes simplex virus 1 entry. *Proc. Natl Acad. Sci. USA* **105**, 10559–10564 (2008).
44. Laine, R. F. et al. Structural analysis of herpes simplex virus by optical super-resolution imaging. *Nat. Commun.* **6**, 5980 (2015).
45. Liu, J., Wright, E. R. & Winkler, H. in *Cryo-EM, Part C: Analyses, Interpretation, and Case studies* Vol. 483 (ed. Jensen, G. J.) 267–290 (Academic, 2010).
46. Park, Y.-G. et al. Protection of tissue physicochemical properties using polyfunctional crosslinkers. *Nat. Biotechnol.* **37**, 73–83 (2019).
47. Neve, R. L., Neve, K. A., Nestler, E. J. & Carlezon, W. A. Use of herpes virus amplicon vectors to study brain disorders. *Biotechniques* **39**, 381–391 (2005).
48. Yu, C.-C. Virus particle analysis. *Github* <https://github.com/jayyu0528/> (2020).
49. Yu, C.-C. Microtubule peak-to-peak distance analysis. *Github* <https://github.com/jayyu0528/> (2020).
50. Yu, C.-C. HSV-1 averaged particle image simulation. *Github* <https://github.com/jayyu0528/> (2020)